## INFORMATION TO USERS

This material was produced from a microfilm copy of the original document. While the most advanced technological means to photograph and reproduce this document have been used, the quality is heavily dependent upon the quality of the original submitted.

The following explanation of techniques is provided to help you understand markings or patterns which may appear on this reproduction.

1. The sign or "target" for pages apparently lacking from the document photographed is "Missing Page(s)". If it was possible to obtain the missing page(s) or section, they are spliced into the film along with adjacent pages. This may have necessitated cutting thru an image and duplicating adjacent pages to insure you complete continuity.

2. When an image on the film is obliterated with a large round black mark, it is an indication that the photographer suspected that the copy may have moved during exposure and thus cause a blurred image. You will find a good image of the page in the adjacent frame.

3. When a map, drawing or chart, etc., was part of the material being photographed the photographer followed a definite method in "sectioning" the material. It is customary to begin photoing at the upper left hand corner of a large sheet and to continue photoing from left to right in equal sections with a small overlap. If necessary, sectioning is continued again — beginning below the first row and continuing on until complete.

4. The majority of users indicate that the textual content is of greatest value, however, a somewhat higher quality reproduction could be made from "photographs" if essential to the understanding of the dissertation. Silver prints of "photographs" may be ordered at additional charge by writing the Order Department, giving the catalog number, title, author and specific pages you wish reproduced.

5. PLEASE NOTE: Some pages may have indistinct print. Filmed as received.

**Xerox University Microfilms**
300 North Zeeb Road
Ann Arbor, Michigan 48106

75-784

RITZ, Charles Louis, 1947-
I) STRUCTURES OF ICl, $ReF_6$, $XeOF_4$ AND $Pt(PF_3)_4$ BY GAS PHASE ELECTRON DIFFRACTION AND II) ELECTRON WAVE HOLOGRAPHY.

The University of Michigan, Ph.D., 1974
Chemistry, physical

**Xerox University Microfilms**, Ann Arbor, Michigan 48106

THIS DISSERTATION HAS BEEN MICROFILMED EXACTLY AS RECEIVED.

# I) STRUCTURES OF ICl, $ReF_6$, $XeOF_4$ AND $Pt(PF_3)_4$ BY GAS PHASE ELECTRON DIFFRACTION AND II) ELECTRON WAVE HOLOGRAPHY

by

Charles Louis Ritz

A dissertation submitted in partial fulfillment
of the requirements for the degree of
Doctor of Philosophy
(Chemistry)
in The University of Michigan
1974

Doctoral Committee:

Professor Lawrence S. Bartell, Chairman
Professor Raoul Kopelman
Associate Professor Donald R. Peacor
Associate Professor Ralph W. Rudolph

To my wife, Susan

## ACKNOWLEDGMENTS

First, I would like to thank Professor Lawrence S. Bartell for his patience, insight and guidance throughout the period I have been at the University of Michigan. I also wish to extend my appreciation to all the members of the electron diffraction group whose valuable assistance in the operation of the diffraction apparatus and analysis of data helped a great deal in the completion of my research.

The research reported in this thesis was supported in part by grants from the National Science Foundation and Horace H. Rackham School of Graduate Studies. Departmental support in the form of a Carpenter Fellowship is gratefully acknowledged. Finally, without a generous allowance from the University of Michigan Computing Center for the use of their facilities, much of this research could not have been carried out.

TABLE OF CONTENTS


| | Page |
|---|---|
| DEDICATION | ii |
| ACKNOWLEDGMENTS | iii |
| LIST OF TABLES | vi |
| LIST OF FIGURES | vii |
| PART I - STRUCTURES OF ICl, $ReF_6$, $XeOF_4$ AND $Pt(PF_3)_4$ BY GAS PHASE ELECTRON DIFFRACTION | 1 |
| INTRODUCTION | 2 |
| ICl STRUCTURE STUDY | |
| A. Introduction | 8 |
| B. Experimental Procedure | 8 |
| C. Treatment of Data | 10 |
| D. Results | 10 |
| $ReF_6$ STRUCTURE STUDY | |
| A. Introduction | 11 |
| B. Reanalysis of Intensity Data for $ReF_6$ | 14 |
| $XeOF_4$ STRUCTURE STUDY | |
| A. Introduction | 16 |
| B. Reanalysis of Intensity Data for $XeOF_4$ | 17 |
| $Pt(PF_3)_4$ STRUCTURE STUDY | |
| A. Introduction | 19 |
| B. Experimental Procedure | 19 |

Page

C. Treatment of Data 21

D. Results 22

REFERENCES - PART I 49

PART II - ELECTRON WAVE HOLOGRAPHY 52

INTRODUCTION 53

EXPERIMENTAL PROCEDURE 56

DISCUSSION OF THEORY 59

REFERENCES - PART II 73

## LIST OF TABLES


| TABLE | | Page |
|---|---|---|
| 1 | Experimental Intensity Data for ICl | 25 |
| 2 | Molecular Parameters and Correlation Coefficients for ICl | 26 |
| 3 | Molecular Parameters and Correlation Coefficients for $ReF_6$ | 36 |
| 4 | Molecular Parameters and Correlation Coefficients for $XeOF_4$ | 42 |
| 5 | Experimental Intensity Data for $Pt(PF_3)_4$ | 44 |
| 6 | Molecular Parameters and Correlation Coefficients for $Pt(PF_3)_4$ | 47 |

## LIST OF FIGURES


| FIGURE | | Page |
|---|---|---|
| 1 | Molecular Intensity Curves for ICl | 28 |
| 2 | Multiple Scattering Correction for $ReF_6$ | 30 |
| 3 | Fourier Sine Transform of Multiple Scattering Correction for $ReF_6$ | 32 |
| 4 | Molecular Intensity Curves for $ReF_6$ | 34 |
| 5 | Fourier Sine Transform of Multiple Scattering Correction for $XeOF_4$ | 38 |
| 6 | Molecular Intensity Curves for $XeOF_4$ | 40 |
| 7 | Molecular Intensity Curves for $Pt(PF_3)_4$ | 45 |
| 8 | Reconstructed Images of Ne and Ar | 66 |
| 9 | Schematic Illustration of Laser Diffractometer | 67 |
| 10 | Schematic Illustration of Microscope | 69 |
| 11 | $\text{Log}_{10}\left[\rho^P(b)/\rho^P(0)\right]^2$ versus b, the Impact Parameter | 71 |

# Part I

# STRUCTURES OF ICl, $ReF_6$, $XeOF_4$ AND $Pt(PF_3)_4$ BY GAS PHASE ELECTRON DIFFRACTION

# INTRODUCTION

Recent advances in electron scattering theory have shown that it is advisable to alter the current routine of data analysis in gas phase electron diffraction when atoms of large atomic numbers ($Z > 40$) are present in the molecules under investigation. The first part of this thesis states the results of investigations on four molecules containing heavy atoms: ICl, $ReF_6$, $XeOF_4$ and $Pt(PF_3)_4$.

First, relevant equations and physical concepts will be presented. In particular, emphasis will be on the incorporation of recent electron scattering theory into routine analysis of data gathered by gas phase electron diffraction.

Gas phase electron diffraction is the electro-optical analogue of light optic Frauenhoffer diffraction. In electron diffraction an electron gun and a magnetic lens replace the light source and dielectric lens of the optical set-up. In light optics, diffraction customarily occurs when light waves are scattered by some barrier placed in their path, whereas in gas phase electron diffraction a 40 kilovolt beam of electrons is diffracted by a gaseous sample.[1]

Intensities of scattered electrons as a function of the scattering angle are recorded on a photographic plate. This set of data is then retrieved from the plate by means of an automated recording microdensitometer.[2]

The resultant intensity which has been obtained from

the photographic record of the scattered electron waves is given by the following formula

$$I_{total}(s) = I_{1\ atom}(s) + I_{2\ atom}(s) + I_{3\ atom}(s)$$

where higher order scattering terms have been neglected. In the above equation, the total intensity, $I_{total}(s)$, is expressed as the sum of a one atom scattering term, $I_{1\ atom}(s)$, a two atom scattering term, $I_{2\ atom}(s)$, and a three atom scattering term, $I_{3\ atom}(s)$.

One atom scattering is analogous to single slit diffraction in the case of light optics. In the present formulation, $I_{1\ atom}(s)$ is given by[3]

$$I_{1\ atom}(s) = K\sum_{i=1}^{N}( |f_i(s)|^2 + (4/a_o^2 s^4)S_i(s)).$$

This represents the contribution to the total intensity of the individual atoms of a particular N atom molecule scattering separately.

In the above equation, K is a constant term dependent on experimental conditions and is of little use in the present treatment, N is the number of atoms in the molecule, $f_i(s)$ is the elastic electron scattering factor for the i th atom, s is the scattering variable equal to $(4\pi/\lambda)\sin(\phi/2)$ where $\lambda$ is the wavelength of the electrons used in the beam and $\phi$ is the angle between the scattered electron and an undeflected electron, S(s) is the inelastic x-ray scattering factor and $a_o$ is the relativistic Bohr radius which is equal to $\hbar^2/2me^2$ where $\hbar$ is Planck's constant divided by $2\pi$, m is the relativistic mass of the electron and e is the charge of the electron.

The one atom intensity falls off very rapidly with in-

creasing values of s. In the limit of the kinematic approximation, $f_i(s)$ can be written as[4]

$$|f_i(s)|^2 = (4/a_o^2 s^4)(Z_i - F_i(s))^2 .$$

The atomic number of atom i is $Z_i$ and its x-ray atomic scattering factor is $F_i(s)$.

In the actual processing of the data, the one atom intensity contribution is readily calculated. Numerous tables and approximate analytical expressions exist for the computation of f(s), F(s) and S(s).[5]

The two atom intensity contribution is given by[6]

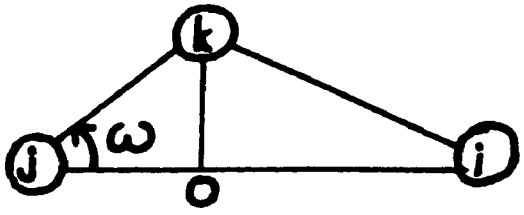
$$I_{2\ atom}(s) = 2K\sum_i^N \sum_j^{N'} |f_i(s)| \cdot |f_j(s)| \cos(\eta_i(s) - \eta_j(s)) \times \int_o^\infty P_{ij}(r)(\sin(sr)/sr)dr$$

and represents the interference between waves scattered by pairs of different atoms. The phase shift of the scattered wave is $\eta(s)$ and the probability that the internuclear distance from the i th and j th atoms lies between r and r + dr is $P_{ij}(r)dr$.

The expression for the three atom intensity is very nearly given by[7]

$$I_{3\ atom}(s) = 2K\sum_i^N \sum_j^N \sum_k^N \mathrm{Re}\{(i/kr_{ij}^2) f_i(s_i) f_j(s_j) \times f_k^*(s)\exp(-1_\perp^2 s^2/2)(1 - 1_\parallel^2 \epsilon(s) s^2) \times J_o(sr_{jk}[1 - \epsilon(s)]\sin\omega_{ijk})\}.$$

The geometry associated with a particular ijk combination is illustrated in the following diagram.



In the preceeding equation, $J_o$ is the Bessel function of zero order, $l_{\parallel}^2$ and $l_{\perp}^2$ are the components of the mean square amplitude of vibration of atom k relative to a point o parallel and perpendicular to $r_{ij}$, and $s_i$, $s_j$ and $\epsilon(s)$ are defined as follows:

$$s_i = |\Lambda| s$$

$$s_j = |1 - \Lambda| s$$

$$\Lambda = (r_{jk}/r_{ij})\cos\omega_{ijk}$$

$$\epsilon = (1/2r_{ij}^2)\{ -f_j''(s_j)/f_j(s_j) + 2f_j'(s_j)f_i'(s_i)/f_j(s_j)f_i(s_i) - f_i''(s_i)/f_i(s_i)\}.$$

The three atom intensity expression corresponds to the fact that the scattering of electrons by any atom pair can be appreciably altered by the presence of a third atom. If this third atom has a high enough atomic number, a significant amount of multiple scattering takes place. Thus for molecules containing an atom or atoms of large atomic number and provided that $\sin\omega$ is sufficiently large, the three atom scattering contribution to the total intensity will be of sufficient magnitude to warrant its inclusion into an accurate analysis of the intensity data.

The three atom scattering term can be looked upon as a correction to the two atom scattering term, $I_{2\ atom}(s)$, since $I_{3\ atom}(s)$ contains no new geometric parameters which are not in some way included in $I_{2\ atom}(s)$. Later in the thesis, details of the effects of $I_{3\ atom}(s)$ will be brought out by the comparison of structure studies which did not include three atom scattering theory and more recent work which took into account the newer theory.

In the least squares analysis of the experimental intensity data, the ratio $I_{total}(s)/I_{1\ atom}(s)$ is used. The rationale for this approach is that the rather well known electron distribution in the molecule is taken into account and one is left with only the problem of unravelling the molecular structure. The result of dividing $I_{total}(s)$ by $I_{1\ atom}(s)$ is to obtain the reduced intensity function, $M(s)$. The reduced molecular intensity function is given by

$$\begin{aligned} M(s) &= \left[I_{total}(s)/I_{1\ atom}(s)\right] - 1 \\ &= \left[I_{2\ atom}(s) + I_{3\ atom}(s)\right] / I_{1\ atom}(s) \\ &= M_{2\ atom}(s) + M_{3\ atom}(s). \end{aligned}$$

$M_{2\ atom}(s)$ and $M_{3\ atom}(s)$ are interpreted to be the contribution to the reduced molecular intensity function by the two and three atom scattering terms respectively.

One is now left with the step of drawing a background function, $I_B(s)$, through the oscillatory intensity data to represent an experimental one atom intensity function, $I_{1\ atom}(s)$. In practice, a more sensitive plot is obtained if the total experimental intensity function, $I_{total}(s)$, is first leveled by dividing it by the theoretical $I_{1\ atom}(s)$. Provided that the electron distribution does not differ much from that corresponding to a superposition of spherical atoms, this $I_B(s)$ should then be smooth and free from any details arising from the electron structure of the atoms making up the molecule.

Specifically, $M_{2\ atom}(s)$ is given by the following formula.[8]

$$M_{2\ atom}(s) = 2\sum_i^N \sum_j^{N'} c_{ij} u_{ij}(s) \cos(\eta_i(s) - \eta_j(s)) \times \int_0^\infty P_{ij}(r)(\sin(sr)/sr)dr$$

where

$$c_{ij} = Z_i Z_j / \sum_k^N (Z_k^2 + Z_k)$$

$$u_{ij}(s) = \{Z_i - F_i(s)\}\{Z_j - F_j(s)\} \sum_i^N (Z_i^2 + Z_i) \times 1/Z_i Z_j \sum_i^N \{[Z_i - F_i(s)]^2 + Z_i S(s)\}.$$

Except for small values of s, $u_{ij}(s)$ is fairly constant and nearly equal to unity for molecules containing only atoms of low atomic number. However, for molecules containing an atom with a large atomic number, $u_{ij}(s)$ can differ considerably from unity.

Since a theoretically reasonable expression for the probability function, $P_{ij}(r)$, does exist, $M_{2\ atom}(s)$ can be summarized as follows:

$$M_{2\ atom}(s) = 2\sum_i^N \sum_j^{N'} c_{ij} u_{ij} \cos(\Delta\eta_{ij}) \exp(-l_{ij}^2 s^2/2) \times \sin\{s[r_{ij} + \phi(s)]\}/sr_{ij}.$$

In the above expression, $l_{ij}^2$ is the mean square amplitude of vibration between the i th and j th atom, $r_{ij}$ is the center of gravity of the radial distribution function $P_{ij}(r)/r$ and $\phi(s)$ is a factor which takes into account the phase shift of the molecular intensity curve from a sine curve at larger s values and is a sensitive measure of the vibrational anharmonicity.[9]

In order to maximize the agreement between theory and experiment and to deduce a structure, a least squares refinement procedure is carried out on the intensity data. The analyses to be reported in this thesis are all based on

least squares treatments of the reduced molecular intensity function.

## ICl STRUCTURE STUDY

### A. Introduction

A study of iodine monochloride was undertaken for two reasons. The first was to examine a simple molecule containing an atom of large atomic number in order to assess the adequacy of one and two atom scattering theory to account for the experimentally observed intensity. When this study was originally undertaken in early 1971, there was no adequate theory to rationalize the disagreement between current theory and experiment in the case where a heavy atom was present in the molecule under investigation.

The second reason for this study was to familiarize the author with the technique of gas phase electron diffraction data analysis. With a simple system, concepts and methods are more easily grasped whereas with a larger and more complicated molecule the fine points are often masked on account of the large numbers of structural parameters and their associated correlations.

### B. Experimental Procedure

The electron diffraction unit used to obtain the raw intensity data was the one located at the University of Michigan. Details of its construction have been discussed before in the literature.[10]

Diffraction patterns produced by the scattered electrons

were recorded on 4" x 5" Kodak Electron Image Plates. In order to compensate for the rapid fall off of intensity with increasing scattering angle, a heart-shaped 48 mm radius rotating sector whose angular opening was proportional to the cube of the sector radius was employed.

Data were taken at two different camera distances; 21 cm and 11 cm. The distance from the center of the .27 mm diameter nozzle tip to the photographic plate was measured with a travelling microscope after each and every experiment.

A sample of ICl was obtained from Mallenkrodt Chemical Company. During the experiment, it was contained in a special glass ampoule and the flow of sample to the diffraction chamber was regulated by a teflon stopcock built into the container. All experiments were performed with the ICl sample at room temperature. The vapor pressure of the sample was never measured due to the compound's extreme reactivity and toxic nature. However, with a beam current of .56 microamps vapor pressure was sufficiently high to produce usable data after 4 seconds exposure for the 21 cm camera distance and roughly 12 seconds for the 11 cm camera distance.

Four plates from the 21 cm camera length and three plates from the 11 cm camera length were selected for analysis. The records of the scattered electron waves were retrieved by a semi-automated recording microdensitometer.[11] The plates were spun about their centers during the microphotometering in order to average out emulsion grains. Readings were taken at .25 mm intervals while scanning completely across the plate

from right to left.

Data from all plates of a particular camera distance were treated separately. From raw voltage data the absorbances, A, were obtained and then converted to exposure, E, by use of the relation:

$$E = A(1 + \alpha_1 A + \alpha_2 A^2 + \alpha_3 A^3)$$

where

$$\alpha_1 = 0.1$$

$$\alpha_2 = 0.133$$

$$\alpha_3 = 0.002$$

C. Treatment of Data

Experimental leveled intensities, $I_o(s)$, were derived from exposures in the conventional manner. Table 1 gives the experimental s, $I_o(s)$, and background function, $I_B(s)$, for each camera distance.

The elastic and inelastic scattering factors and phase shifts computed by Schafer, Yates and Bonham[12] were used throughout the analysis.

The determination of the bond length and mean square amplitude of vibration for ICl was done by a least squares refinement procedure on the intensity data. At first, the data for each camera distance were treated individually. After a suitable background had been determined, the data from both camera distances were allowed to combine and overlap so as to form a composite reduced molecular intensity function extending over the range $4.5\ \text{Å}^{-1} \leqslant s \leqslant 38.3\ \text{Å}^{-1}$.

D. Results of Study on ICl

The final values of the bond length and mean square amplitude of vibration are listed in Table 2 along with the results of earlier spectroscopic investigations by other workers.[13,28] In Figure 1, the experimental and theoretical reduced molecular intensity function and their difference are illustrated.

In order to calculate the $r_g$ bondlength listed in Table 1 from the spectroscopic equilibrium bond length, $r_e$, given by Townes[13] the following formula was used[9]

$$r_g = r_e + 3al_\alpha^2/2 + 13a^3l_\alpha^4/12$$

where a is the anharmonicity and $l_\alpha^2$ is the root mean-square amplitude of vibration reckoned from the equilibrium position, $r_e$, and can be given for a diatomic molecule by the formula[9]

$$l_\alpha^2 = h/8\pi^2\mu\omega_e.$$

In the above equation, h is Planck's constant, $\mu$ is the reduced mass of the molecule and $\omega_e$ is the vibrational frequency. The value for $\omega_e$ is listed by Herzberg[28] and $l_g^2$ can be easily calculated by using the following expression.[9]

$$l_g^2 = l_\alpha^2 + 3a^2l_\alpha^4/2 - 59a^4l_\alpha^6/32.$$

From Figure 1, it is seen that the agreement between theory and experiment is good. Therefore one and two atom scattering theory is adequate to account for the data.

## $ReF_6$ STRUCTURE STUDY

### A. Introduction

In order to examine the applicability of the three atom

scattering theory to routine analysis, to test the theory's accuracy and to investigate the sensitivity of derived molecular parameters to inclusion of this correction, the structure of rhenium hexafluoride was redetermined. The reason $ReF_6$ was chosen was that it contained a heavy atom and possessed simple octahedral symmetry. Furthermore, up to that time, no complete molecular structure determination had been carried out using a least squares refinement which took into account three atom scattering.

Spectroscopic evidence indicated $O_h$ symmetry[14] for $ReF_6$ and previous work by Jacob and Bartell[15] on the gas phase electron diffraction data, which did not take into account three atom scattering, also indicated an octahedral symmetry. Thus the only geometric parameter needed to define the structure completely was the Re-F bond length.

When the structure was initially done by Jacob using an $O_h$ model, certain discrepancies appeared when a detailed comparison was made between the theoretical and experimental reduced molecular intensity functions. At that time, it was not known what was responsible for these systematic inconsistencies which were observed to have a periodicity roughly corresponding to $\cos(sr_{Re-F})$.

After they had derived an analytical expression for the three atom scattering, Wong and Bartell[16] examined the cosine component associated with the zeroth order Bessel function occuring in the three atom intensity formula in as much as

$$J_o(x) \cong (1/\sqrt{\pi x})(\sin(x) + \cos(x))$$

where in this case

$$x = sR_{jk}(1 - \epsilon(s))\sin\omega$$

They reasoned that the largest single contributing ijk combination occuring in the three atom expression was the configuration corresponding to I in the following diagram.




For configuration I, $\omega$ equals $90^{o}$. Thus the argument of $J_o$ is nearly equal to $sR_{jk}$ since the $(1 - \epsilon(s))$ term is almost unity within the range of the experimentally obtained intensity data. Because the two atom electron scattering term already contains a sin(sr) term for the Re-F bond length it was plausible to assume that the scale factor in Jacob's original structure determination, which took into account only one and two atom scattering terms, had already partially absorbed the sine component of the zeroth order Bessel function which occurs in the expression for the three atom scattering. Since the sine term was at least partially absorbed in the conventional analysis, this left only the $\cos(sr_{jk})$ term which showed up in the earlier work as a close approximation to the observed difference between theory and experiment.

There is however another ijk combination which calculations show contributes a significant amount to the three atom intensity. That configuration corresponds to II in the pre-

ceding diagram. For II, the sine term is not absorbed in a systematic way in the conventional analysis because the $sR_{jk}$ sin$\omega$ term (equal to ½ the F--F distance in this case) does not correspond to any bonded or non-bonded distance.

The three atom contribution of configurations I and II to the reduced molecular intensity function (with the sine term for I suppressed) is plotted in Figure 2. Also drawn on the same graph is the difference between theory and experiment as observed by Jacob. The agreement between the two curves is good and is evidence that the three atom theory can at least, in the case of $ReF_6$, account for the earlier irregularities observed between theory and experiment.

The Fourier sine transform of the calculated three atom scattering contribution (with the sine term for I suppressed) is plotted in Figure 3. On the same graph is the previously obtained experimentally observed residual - the difference between the theoretical and the experimental radial distribution function.

B. Reanalysis of the Intensity Data for $ReF_6$

Although the calculated three atom contribution closely resembled the previously obtained residuals in the reduced molecular intensity function and radial distribution function the comparisons in Figures 2 and 3 suppressing the $\sin(sr_{Re-F})$ term cannot be rigorous because the two atom and three atom sine terms are modulated quite differently by atomic phase shifts. Therefore a decision was made to reexamine the previously gathered intensity data. With this data, a new

analysis was performed which included the three atom theory from the very beginning.

Previous work on $ReF_6$ indicated that Bonham and Ukaji phase shifts,[17] Heisenberg and Bewilogua inelastic scattering factors[18] and $|f_{Re}(s)|$ and $|f_F(s)|$ given by Bonham and Cox[19] were suitable. However for the current work, the scattering factors computed by Schafer, Yates and Bonham[20] were found to be satisfactory.

A least squares method was employed to determine the molecular parameters giving the best fit between experimental and calculated intensities. A current program used in least squares analysis was modified to include three atom scattering theory.

A new but not significantly different background function, $I_B(s)$, was obtained for the 21 cm and 11 cm camera lengths previously reported by Bartell and Jacob. After a suitable background function had been obtained, both sets of data were blended to form a composite experimental reduced molecular intensity function extending over the range $5.3\ \text{Å}^{-1} \leqslant s \leqslant 39.3\ \text{Å}^{-1}$.

Throughout the least squares analysis, an octahedral geometry was assumed. The number of independent parameters used to characterize the structure was four; the Re-F bond length and the mean square amplitudes of vibration which correspond to to the Re-F bond length and the two distinct F--F non-bonded distances. The final values of these four parameters are listed in Table 3 along with values obtained in the earlier work and results from infrared spectroscopy.

In the second part of Table 3, the correlation coefficients for the derived molecular parameters are listed. In Figure 4, the experimental and theoretical reduced molecular intensity functions are plotted along with their differnce. Also included in this graph for comparison is the observed residual intensity curve obtained by Jacob.

The new values assigned to the structural parameters differ little from those determined by Jacob and Bartell. It is however interesting to note the change in the mean square amplitudes of vibration for the non-bonded distances. These are now closer to those values computed from infrared vibrational frequencies. Besides improving the agreement between theory and experiment, it appears that the inclusion of the newer three atom scattering theory allows one to make more accurate comparisons of electron diffraction and spectroscopic mean square amplitudes of vibration.

## $XeOF_4$ STRUCTURE STUDY

### A. Introduction

Another molecule which was examined in detail was $XeOF_4$. Since this molecule contains an atom of relatively large atomic number, it was thought that the contribution to the total intensity due to the three atom scattering would be of sufficient magnitude so as to be actually observed.

Using the technique of gas phase electron diffraction, Jacob and Bartell determined the structure of $XeOF_4$.[21] They analyzed the diffraction data without the benefit of any theory to help account for the unusual nature of the residual

in the radial distribution function. In Figure 5, this residual curve is plotted along with the Fourier sine transform of the calculated three atom intensity (only the cosine component present in some ijk combinations, see Appendix).

The agreement between the two curves illustrated in Figure 5 is not perfect. However, it is an indication that the current multiple scattering theory would be able to account for at least a part of the disagreement between the experimental and Jacob's calculated intensity. Therefore the decision was made to reexamine the previously gathered data. With this data, a new analysis was performed which included three atom scattering from the very beginning.

B. Reanalysis of Intensity Data for $XeOF_4$

Intensity data to be reexamined was that originally obtained by Jacob. In this reanalysis, data from two camera distances was utilized; the 21 cm long camera distance and 11 cm middle camera distance.

The scattering factors used were those calculated by Schafer, Yates and Bonham.[22] Care was taken to insure that the scattering factors were smooth as a function of s. This meant that the results of the computer programs used to generate the first and second derivatives of the elastic scattering factor were closely examined for unusual changes in sign. This scrutiny was required since these derivatives were fed into calculations for the three atom scattering correction term, $\epsilon(s)$.

As with $ReF_6$, a new but not significantly different

background function, $I_B(s)$, was obtained for the 21 cm and 11 cm camera distances previously reported by Jacob and Bartell. After a suitable background function had been obtained, both sets of data were blended to form a composite experimental reduced molecular intensity function extending over the range $6.9\ \text{Å}^{-1} \leq s \leq 36.4\ \text{Å}^{-1}$.

The number of geometric parameters needed for defining the structure is three; the Xe-O and Xe-F bond lengths and the O-Xe-F angle. This choice of parameters is consistent with the geometrical constraint of 4-fold symmetry around the axis defined by the Xe-O bond. The final values of these parameters are listed in Table 4 along with the values obtained in the earlier diffraction work (using electron diffraction alone) and results from microwave spectroscopy.[23] In the second part of Table 4, the correlation coefficients for the derived molecular parameters are listed. In Figure 6, the experimental and theoretical reduced molecular intensity functions are plotted along with their difference. Also included in this graph for comparison is the observed residual intensity curve obtained by Jacob in the earlier work.

As shown in Table 4, the results of the new analysis which included three atom scattering calculations indicate a structure which differs little from that obtained earlier. As was observed for $ReF_6$, the mean square amplitudes of vibration for the non-bonded atom pairs are closer to those computed from a study of microwave frequencies. Though

improving to a small extent the appearance of the $\Delta sM(s)$ curve, inclusion of the newer theory again allows one to make more accurate comparisons of the electron diffraction and spectroscopic mean square amplitudes of vibration.

## $Pt(PF_3)_4$ STRUCTURE STUDY

### A. Introduction

After a study of $ReF_6$ and $XeOF_4$ was completed, a new molecule of non-octahedral symmetry was wanted in order to further test three atom scattering theory. $Pt(PF_3)_4$ was chosen because it had an atom of relatively large atomic number, an obvious non-octahedral geometry, a very high vapor pressure at room temperature and was available from a commercial source in a pure state.

The determination of the structure from the intensity data was done two times. In the first analysis of the data, no three atom scattering was included in the calculation of the theoretical reduced molecular intensity function. In the second analysis of the same data, three atom scattering corrections were included. The basis of the current study was to test whether or not the inclusion of multiple scattering corrections significantly improved the agreement between theory and experiment and to determine its effect on the derived molecular parameters.

### B. Experimental Procedure

The electron diffraction unit used to obtain the raw intensity data was the one located at the University of Michigan. Details of its construction have been discussed

elsewhere in the literature.[24]

Diffraction patterns produced by the scattered electrons were recorded on 4" x 5" Kodak Electron Image Plates. In order to compensate for the rapid fall off of intensity with increasing scattering angle, a 44mm radius heart-shaped sector whose angular opening was proportional to the cube of the sector radius was employed.

Data were collected at two different camera lengths; 21 cm and 11 cm. The distance from the .27 mm diameter nozzle tip to the photographic plate was measured with a traveling microscope.

A sample of $Pt(PF_3)_4$ was obtained from Pressure Chemical Company. The purity of the sample was given by the manufacturer to be at least 98% with the remaining being made up of arsenic dissolved in the liquid $Pt(PF_3)_4$. No further check of sample purity was made.

During the experiment, the compound was contained in a glass bulb equipped with a cold finger and ground glass stopcock joints. The flow of sample was regulated by a Monel valve located between the glass bulb and the diffraction chamber. All experiments were performed with the $Pt(PF_3)_4$ sample contained in the cold finger of the glass bulb at a temperature of $-30^{o}C$. This temperature was held constant by keeping the cold finger suspended in a bromobenzene slush bath.

The vapor pressure of $Pt(PF_3)_4$ at $-30^{o}$ C was measured directly over mercury and was found to be approximately 4 mm.

This vapor pressure was sufficiently high to produce good data after 16 seconds exposure for the 21 cm camera length and 60 seconds exposure for the 11 cm camera length for a beam current of .56 microamperes.

Three plates from the long camera distance and four from the middle camera distance were selected for analysis. The records of the scattered electron waves were retrieved by a semi-automated recording microdensitometer.[25] The plates were spun about their centers during the microphotometering in order to average out emulsion grains. Readings were taken at .25 mm intervals while scanning completely across the plate from right to left.

Data from all plates of a particular camera distance were treated separately. From the raw voltage data, absorbances, A, were obtained and then converted to exposures, E, by use of the following relation.

$$E = A(1 + \alpha_1 A + \alpha_2 A^2 + \alpha_3 A^3)$$

where

$$\alpha_1 = 0.1$$

$$\alpha_2 = 0.01333$$

$$\alpha_3 = 0.002$$

C. Treatment of Data

Experimental leveled intensities, $I_o(s)$, were derived from exposures in the conventional manner. Table 5 gives the experimental s, $I_o(s)$ and background function, $I_B(s)$, for each camera distance. The background functions for the two camera distances were kept constant during the structure

determinations.

The elastic and inelastic scattering factors and phase shifts calculated by Schafer, Yates and Bonham[22] were used throughout the analysis. Care was taken to insure that the elastic scattering factors were smooth as a function of s. This meant that the output of the computer programs used to generate the first and second derivatives of the scattering factors were closely examined for unusual changes in sign. This scrutiny is required since these derivatives are used in the calculation of the three atom scattering correction term, $\epsilon(s)$.

The determination of the bond length and mean square amplitudes of vibration for $Pt(PF_3)_4$ was done by a least squares refinement procedure on the intensity data. At first the data for each camera distance were treated individually. After a suitable background had been determined, the data from both camera distances were allowed to combine and overlap to form a composite reduced molecular intensity function extending over the range $6.6\ \text{Å}^{-1} \leqslant s \leqslant 39.3\ \text{Å}^{-1}$.

D. Results

The final values of the bond lengths and mean square amplitudes of vibration derived from both structure studies are listed in Table 6. In Figure 7, the experimental and theoretical reduced molecular intensity functions are plotted for that structure determination which included three atom scattering corrections. However, the sM(s) function for both studies in included for comparison.

No attempt was made to determine the barrier of rotation for the tetrahedrally oriented $PF_3$ groups with respect to each other. The present compound was assumed analogous to $Ni(PF_3)_4$. When the latter's structure was determined by gas phase electron diffraction, essentially free rotation of the $PF_3$ groups was found.[26] For $Ni(PF_3)_4$, the computation of the scattering from a freely rotating model was done by adding up contributions from configurations obtained by rotating the $PF_3$ groups in steps of $15^o$.

In the current study, the $PF_3$ groups were assigned a tetrahedral orientation about the central Pt atom and were not allowed to rotate. They were initially given a twist about the Pt-P bond which gave a spectrum of long F--F and long P--F distances whose spread was similar to that calculated for the rotation of the $PF_3$ groups in $15^o$ increments. Assigning values from .2 Å to .5 Å for the long F--F distance root mean square amplitude of vibration had no noticeable effect on the agreement between theory and experiment. Thus this particular vibration was given the value of .2 Å for both structure determinations.

The results of this study do not differ significantly from those obtained by Marriot, Salthouse and Ware who also determined the structure of $Pt(PF_3)_4$ by gas phase electron diffraction.[27] These researchers used only one and two atom scattering and no multiple scattering corrections. For the Pt-P and P-F bond lengths they reported 2.230 Å and 1.546 Å respectively and $98.9^o$ for the F-P-F angle. In the current

study these parameters were found to be 2.229 Å for the Pt-P bond length, 1.551 Å for the P-F bond length and 98.6° for the F-P-F angle.

From Table 6, it is seen that the multiple scattering corrections are small and of the magnitude of the noise in the data. Including the corrections in the analysis does bring experiment into better agreement with theory by a small amount, however. The molecular parameters are the same in both of the studies except for changes in amplitudes of vibration of several of the non-bonded distances.

TABLE 1

21 cm Camera Distance Intensity Data For IC1 ($R^3$ Sector)

| s | $I_o(s)$ | $I_B(s)$ | s | $I_o(s)$ | $I_B(s)$ | s | $I_o(s)$ | $I_B(s)$ | s | $I_o(s)$ | $I_B(s)$ |
|---|---|---|---|---|---|---|---|---|---|---|---|
| 4.135 | 0.2170 | | 0.562 | 0.3572 | 0.1870 | 12.955 | 0.0933 | 0.1786 | 17.296 | 0.2329 | 0.2078 |
| 4.259 | 0.1207 | | 0.685 | 0.3736 | 0.1865 | 13.076 | 0.1105 | 0.1784 | 17.416 | 0.2246 | 0.2090 |
| 4.382 | 0.0057 | 0.3548 | 0.807 | 0.3711 | 0.1862 | 13.198 | 0.1254 | 0.1782 | 17.535 | 0.2141 | 0.2102 |
| 4.505 | 7.9298 | 0.3493 | 0.930 | 0.3522 | 0.1861 | 13.319 | 0.1431 | 0.1780 | 17.655 | 0.2071 | 0.2114 |
| 4.628 | 7.8804 | 0.3437 | 9.052 | 0.3272 | 0.1860 | 13.440 | 0.1651 | 0.1779 | 17.775 | 0.1977 | 0.2126 |
| 4.752 | 7.9133 | 0.3380 | 9.175 | 0.2853 | 0.1859 | 13.561 | 0.1864 | 0.1776 | 17.894 | 0.1900 | 0.2137 |
| 4.875 | 7.9346 | 0.3323 | 9.297 | 0.2448 | 0.1858 | 13.682 | 0.2065 | 0.1774 | 18.014 | 0.1874 | 0.2149 |
| 4.998 | 7.9896 | 0.3264 | 9.420 | 0.1979 | 0.1856 | 13.804 | 0.2210 | 0.1773 | 18.133 | 0.1856 | 0.2161 |
| 5.121 | 0.0703 | 0.3204 | 9.542 | 0.1538 | 0.1853 | 13.925 | 0.2327 | 0.1774 | 18.252 | 0.1888 | 0.2173 |
| 5.244 | 0.1715 | 0.3143 | 9.664 | 0.1117 | 0.1850 | 14.046 | 0.2374 | 0.1778 | 18.372 | 0.1928 | 0.2184 |
| 5.367 | 0.2815 | 0.3081 | 9.787 | 0.0817 | 0.1847 | 14.167 | 0.2458 | 0.1785 | 18.491 | 0.1971 | 0.2196 |
| 5.491 | 0.3830 | 0.3019 | 9.909 | 0.0580 | 0.1845 | 14.288 | 0.2433 | 0.1795 | 18.610 | 0.2005 | 0.2208 |
| 5.614 | 0.4649 | 0.2955 | 10.031 | 0.0469 | 0.1843 | 14.408 | 0.2366 | 0.1806 | 18.729 | 0.2101 | 0.2219 |
| 5.737 | 0.5114 | 0.2889 | 10.153 | 0.0392 | 0.1841 | 14.529 | 0.2219 | 0.1817 | 18.848 | 0.2170 | 0.2231 |
| 5.860 | 0.5809 | 0.2822 | 10.275 | 0.0556 | 0.1839 | 14.650 | 0.2084 | 0.1828 | 18.967 | 0.2253 | 0.2242 |
| 5.983 | 0.5927 | 0.2753 | 10.398 | 0.0745 | 0.1837 | 14.771 | 0.1971 | 0.1838 | 19.086 | 0.2315 | 0.2254 |
| 6.106 | 0.6004 | 0.2682 | 10.520 | 0.1003 | 0.1835 | 14.892 | 0.1782 | 0.1849 | 19.205 | 0.2401 | 0.2265 |
| 6.229 | 0.5585 | 0.2611 | 10.642 | 0.1343 | 0.1832 | 15.012 | 0.1639 | 0.1860 | 19.324 | 0.2432 | 0.2276 |
| 6.352 | 0.5090 | 0.2540 | 10.764 | 0.1728 | 0.1830 | 15.133 | 0.1524 | 0.1871 | 19.443 | 0.2457 | 0.2287 |
| 6.475 | 0.4359 | 0.2471 | 10.886 | 0.2052 | 0.1827 | 15.254 | 0.1485 | 0.1882 | 19.561 | 0.2457 | 0.2299 |
| 6.598 | 0.3516 | 0.2403 | 11.008 | 0.2395 | 0.1825 | 15.374 | 0.1377 | 0.1893 | 19.680 | 0.2501 | 0.2310 |
| 6.721 | 0.2610 | 0.2336 | 11.130 | 0.2623 | 0.1822 | 15.495 | 0.1383 | 0.1904 | 19.799 | 0.2475 | 0.2606 |
| 6.844 | 0.1802 | 0.2273 | 11.252 | 0.2836 | 0.1820 | 15.615 | 0.1433 | 0.1916 | 19.917 | 0.2627 | 0.6931 |
| 6.967 | 0.1040 | 0.2212 | 11.374 | 0.2936 | 0.1817 | 15.735 | 0.1490 | 0.1927 | 20.036 | 0.2469 | 0.6588 |
| 7.090 | 7.9580 | 0.2156 | 11.496 | 0.2939 | 0.1814 | 15.856 | 0.1591 | 0.1938 | 20.154 | 0.2477 | |
| 7.212 | 7.9568 | 0.2104 | 11.617 | 0.2866 | 0.1812 | 15.976 | 0.1703 | 0.1950 | 20.272 | 0.2532 | |
| 7.335 | 7.9739 | 0.2059 | 11.739 | 0.2656 | 0.1809 | 16.096 | 0.1865 | 0.1961 | 20.391 | 0.2536 | |
| 7.458 | 7.9706 | 0.2020 | 11.861 | 0.2419 | 0.1807 | 16.217 | 0.2007 | 0.1973 | 20.509 | 0.2541 | |
| 7.581 | 7.9890 | 0.1987 | 11.983 | 0.2160 | 0.1804 | 16.337 | 0.2164 | 0.1984 | 20.627 | 0.2506 | |
| 7.704 | 0.0194 | 0.1961 | 12.104 | 0.1843 | 0.1802 | 16.457 | 0.2292 | 0.1996 | 20.745 | 0.2511 | |
| 7.826 | 0.0600 | 0.1940 | 12.226 | 0.1606 | 0.1799 | 16.577 | 0.2378 | 0.2008 | 20.863 | 0.2576 | |
| 7.949 | 0.1150 | 0.1922 | 12.347 | 0.1355 | 0.1797 | 16.697 | 0.2382 | 0.2019 | 20.981 | 0.2668 | |
| 8.072 | 0.1732 | 0.1907 | 12.469 | 0.1155 | 0.1795 | 16.817 | 0.2468 | 0.2031 | 21.099 | 0.2750 | |
| 8.194 | 0.2355 | 0.1895 | 12.591 | 0.1003 | 0.1792 | 16.937 | 0.2459 | 0.2043 | 21.217 | 0.2873 | |
| 8.317 | 0.2848 | 0.1884 | 12.712 | 0.0916 | 0.1790 | 17.057 | 0.2448 | 0.2055 | 21.335 | 0.3035 | |
| 8.440 | 0.3260 | 0.1876 | 12.833 | 0.0908 | 0.1788 | 17.176 | 0.2438 | 0.2066 | | | |

11 cm Camera Distance Intensity Data For IC1 ($R^3$ Sector)

| s | $I_o(s)$ | $I_B(s)$ | s | $I_o(s)$ | $I_B(s)$ | s | $I_o(s)$ | $I_B(s)$ | s | $I_o(s)$ | $I_B(s)$ |
|---|---|---|---|---|---|---|---|---|---|---|---|
| 8.430 | 17.4955 | | 16.737 | 17.3963 | 17.3143 | 24.811 | 17.3591 | 17.3552 | 32.557 | 17.5508 | 17.5394 |
| 8.663 | 17.5704 | | 16.965 | 17.4028 | 17.3146 | 25.031 | 17.3598 | 17.3583 | 32.766 | 17.5582 | 17.5453 |
| 8.896 | 17.6207 | | 17.193 | 17.3732 | 17.3150 | 25.251 | 17.3705 | 17.3615 | 32.976 | 17.5599 | 17.5512 |
| 9.129 | 17.5831 | | 17.421 | 17.3477 | 17.3154 | 25.470 | 17.3622 | 17.3649 | 33.185 | 17.5633 | 17.5572 |
| 9.361 | 17.4395 | | 17.648 | 17.3119 | 17.3160 | 25.689 | 17.3636 | 17.3685 | 33.394 | 17.5582 | 17.5632 |
| 9.594 | 17.2677 | | 17.875 | 17.2783 | 17.3165 | 25.908 | 17.3731 | 17.3724 | 33.602 | 17.5719 | 17.5692 |
| 9.826 | 17.1462 | | 18.102 | 17.2572 | 17.3170 | 26.127 | 17.3706 | 17.3766 | 33.810 | 17.5813 | 17.5753 |
| 10.059 | 17.0775 | | 18.329 | 17.2586 | 17.3175 | 26.345 | 17.3770 | 17.3809 | 34.018 | 17.5795 | 17.5815 |
| 10.291 | 17.1550 | | 18.555 | 17.2724 | 17.3178 | 26.564 | 17.3782 | 17.3855 | 34.226 | 17.5919 | 17.5877 |
| 10.523 | 17.2554 | | 18.782 | 17.2985 | 17.3183 | 26.781 | 17.3826 | 17.3902 | 34.433 | 17.6011 | 17.5939 |
| 10.755 | 17.3252 | 17.3686 | 19.008 | 17.3244 | 17.3187 | 26.999 | 17.3908 | 17.3951 | 34.640 | 17.6067 | 17.6001 |
| 10.987 | 17.4807 | 17.3720 | 19.234 | 17.3574 | 17.3192 | 27.216 | 17.4013 | 17.4001 | 34.846 | 17.6086 | 17.6064 |
| 11.218 | 17.5889 | 17.3763 | 19.460 | 17.3607 | 17.3197 | 27.433 | 17.4071 | 17.4052 | 35.052 | 17.6111 | 17.6127 |
| 11.450 | 17.5906 | 17.3809 | 19.685 | 17.3579 | 17.3203 | 27.650 | 17.4129 | 17.4104 | 35.258 | 17.6150 | 17.6190 |
| 11.682 | 17.6152 | 17.3850 | 19.911 | 17.3605 | 17.3209 | 27.867 | 17.4160 | 17.4157 | 35.464 | 17.6224 | 17.6254 |
| 11.913 | 17.5313 | 17.3879 | 20.136 | 17.3448 | 17.3216 | 28.083 | 17.4257 | 17.4211 | 35.669 | 17.6222 | 17.6317 |
| 12.144 | 17.4120 | 17.3890 | 20.361 | 17.3225 | 17.3224 | 28.299 | 17.4262 | 17.4266 | 35.874 | 17.6287 | 17.6381 |
| 12.375 | 17.2972 | 17.3873 | 20.585 | 17.3121 | 17.3233 | 28.515 | 17.4337 | 17.4321 | 36.079 | 17.6347 | 17.6445 |
| 12.606 | 17.2209 | 17.3826 | 20.810 | 17.2978 | 17.3242 | 28.730 | 17.4474 | 17.4376 | 36.283 | 17.6383 | 17.6509 |
| 12.837 | 17.1746 | 17.3750 | 21.034 | 17.3009 | 17.3250 | 28.945 | 17.4553 | 17.4432 | 36.487 | 17.6452 | 17.6573 |
| 13.068 | 17.2067 | 17.3658 | 21.258 | 17.3059 | 17.3259 | 29.160 | 17.4495 | 17.4488 | 36.691 | 17.6536 | 17.6636 |
| 13.298 | 17.2628 | 17.3561 | 21.482 | 17.3183 | 17.3268 | 29.374 | 17.4557 | 17.4544 | 36.894 | 17.6569 | 17.6700 |
| 13.529 | 17.3519 | 17.3464 | 21.706 | 17.3300 | 17.3278 | 29.589 | 17.4518 | 17.4600 | 37.097 | 17.6648 | 17.6764 |
| 13.759 | 17.1606 | 17.3370 | 21.929 | 17.3366 | 17.3289 | 29.803 | 17.4571 | 17.4657 | 37.299 | 17.6707 | 17.6828 |
| 13.989 | 17.4490 | 17.3293 | 22.152 | 17.3455 | 17.3300 | 30.016 | 17.4468 | 17.4713 | 37.502 | 17.6823 | 17.6892 |
| 14.219 | 17.4532 | 17.3238 | 22.375 | 17.3421 | 17.3313 | 30.230 | 17.4688 | 17.4769 | 37.704 | 17.7103 | 17.6955 |
| 14.449 | 17.4279 | 17.3202 | 22.598 | 17.3436 | 17.3327 | 30.443 | 17.4742 | 17.4825 | 37.905 | 17.7153 | 17.7018 |
| 14.678 | 17.3682 | 17.3177 | 22.820 | 17.3444 | 17.3343 | 30.655 | 17.4795 | 17.4881 | 38.106 | 17.7319 | 18.5076 |
| 14.908 | 17.3035 | 17.3159 | 23.042 | 17.3271 | 17.3360 | 30.868 | 17.4833 | 17.4937 | 38.307 | 17.7388 | 18.0556 |
| 15.137 | 17.2334 | 17.3146 | 23.264 | 17.3219 | 17.3378 | 31.080 | 17.4926 | 17.4993 | 38.508 | 17.7358 | |
| 15.366 | 17.2058 | 17.3136 | 23.486 | 17.3235 | 17.3397 | 31.292 | 17.5133 | 17.5050 | 38.708 | 17.7487 | |
| 15.595 | 17.2142 | 17.3131 | 23.707 | 17.3275 | 17.3419 | 31.503 | 17.5148 | 17.5106 | 38.908 | 17.7665 | |
| 15.824 | 17.2325 | 17.3129 | 23.929 | 17.3337 | 17.3442 | 31.715 | 17.5292 | 17.5163 | 39.108 | 17.7975 | |
| 16.053 | 17.2737 | 17.3131 | 24.150 | 17.3460 | 17.3466 | 31.926 | 17.5337 | 17.5220 | | | |
| 16.281 | 17.3317 | 17.3135 | 24.370 | 17.3495 | 17.3493 | 32.136 | 17.5399 | 17.5278 | | | |
| 16.509 | 17.3622 | 17.3139 | 24.591 | 17.3466 | 17.3521 | 32.347 | 17.5472 | 17.5336 | | | |

TABLE 2

A. MOLECULAR PARAMETERS FOR ICl

| | Current Study | Spectroscopy[b] |
|---|---|---|
| $r_g$(I-Cl), Å | 2.325(9)[c] | 2.3208 |
| $l_g$(I-Cl), Å | 0.049(12) | 0.045 |
| $\sigma(I_o)/\bar{I}_o$[a] | 0.0006 | |

B. CORRELATION COEFFICIENTS FOR ICl[d]

| | $r_g$(I-Cl) | $l_g$(I-Cl) | R |
|---|---|---|---|
| $r_g$(I-Cl) | 1 | -0.08 | -0.07 |
| $l_g$(I-Cl) | | 1 | 0.70 |
| R[e] | | | 1 |

a) The sigma of intensity is based on a weighting of the intensity data proportional to $s^2$.

b) The bond length is taken from Townes[13] and the vibration parameter is based on data given in a table compiled by Herzberg.[28] Both of these molecular parameters are adjusted so as to be put on the same basis as the diffraction results by a method discussed in the text.

c) All estimated uncertainties include random and systematic errors and correspond to $2.5\sigma$ where $\sigma$ is the standard deviation. Systematic errors for wavelength and camera distance measurement and radial measurement in microphotometer scanning are estimated to be 3, 3 and 2 parts per ten thousand respectively.

d) Matrix elements are given by

TABLE 2 (continued)

$$\rho_{ij} = (M_x^W)_{ij} / [(M_x^W)_{ii}(M_x^W)_{jj}]^{\frac{1}{2}}$$

where $M_x^W$ is the bona fide error matrix.

e) Index of resolution; dimensionless and equal to .87 and .84 for the long and short camera distances respectively.

Figure 1 Molecular intensity curves for ICl.

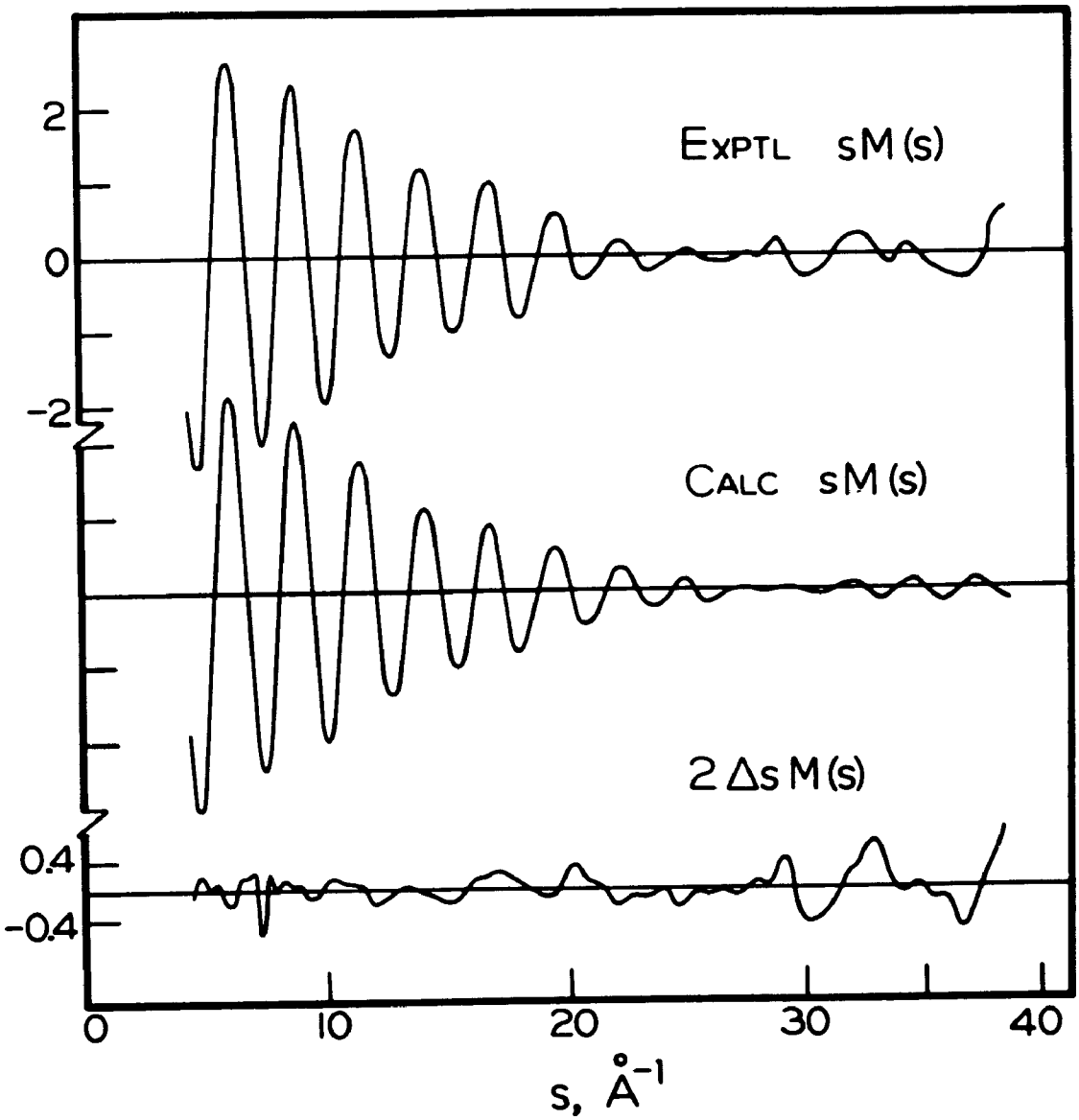

2
0
-2
EXPTL sM(s)
CALC sM(s)
2 Δs M(s)
0.4
-0.4
0
10
20
30
40
s, Å$^{-1}$

Figure 2 Calculated multiple scattering contribution to the reduced molecular intensity function for $ReF_6$ (dashed line) and the $\Delta M(s)$ which was obtained by Jacob and Bartell.

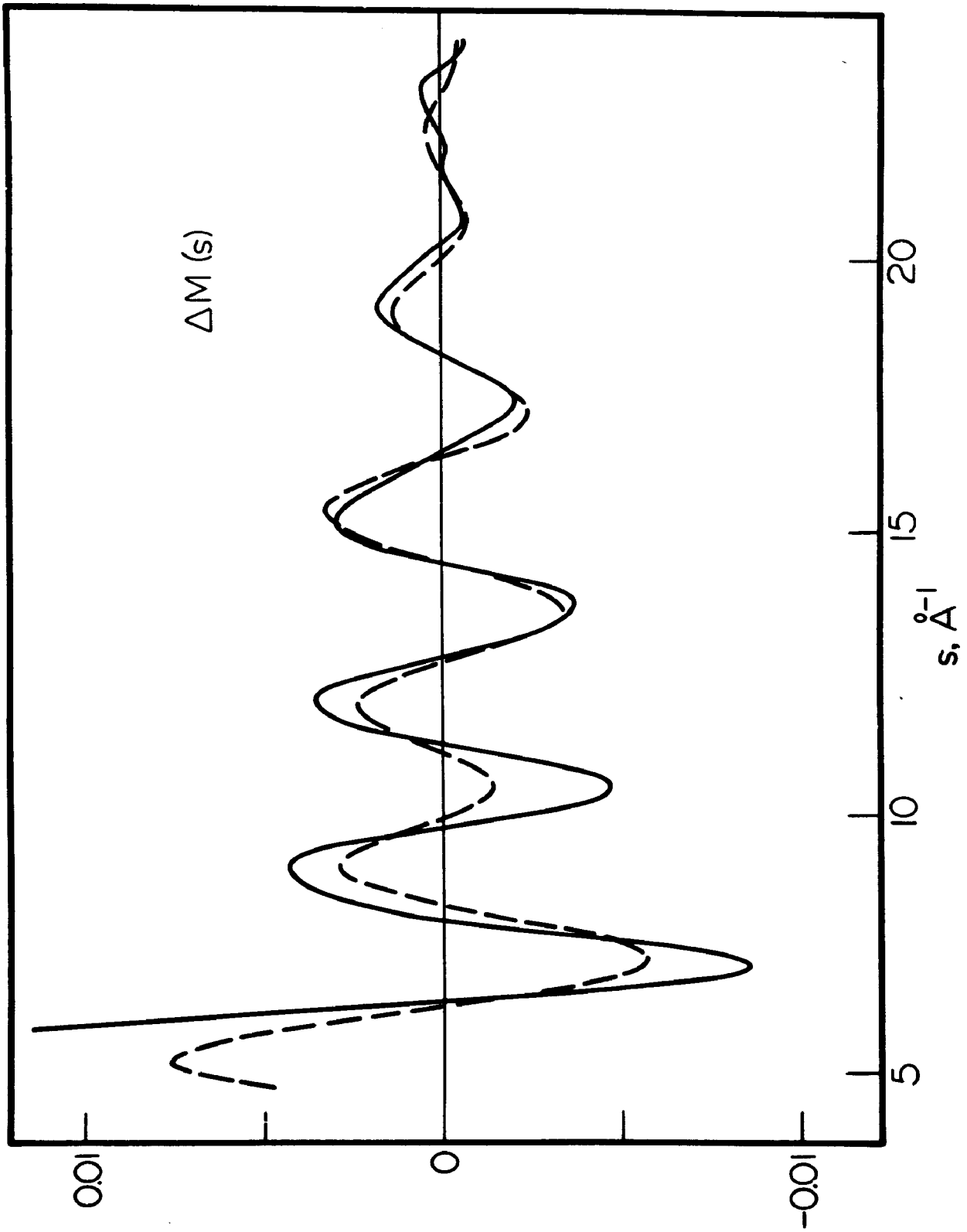

ΔM (s)
0.01
0
-0.01
5
10
15
20
s, Å⁻¹

Figure 3 Fourier sine transform of the calculated multiple scattering contribution to the reduced molecular intensity function for $ReF_6$ (dashed line) and the radial distribution function along with its residual observed by Jacob and Bartell.

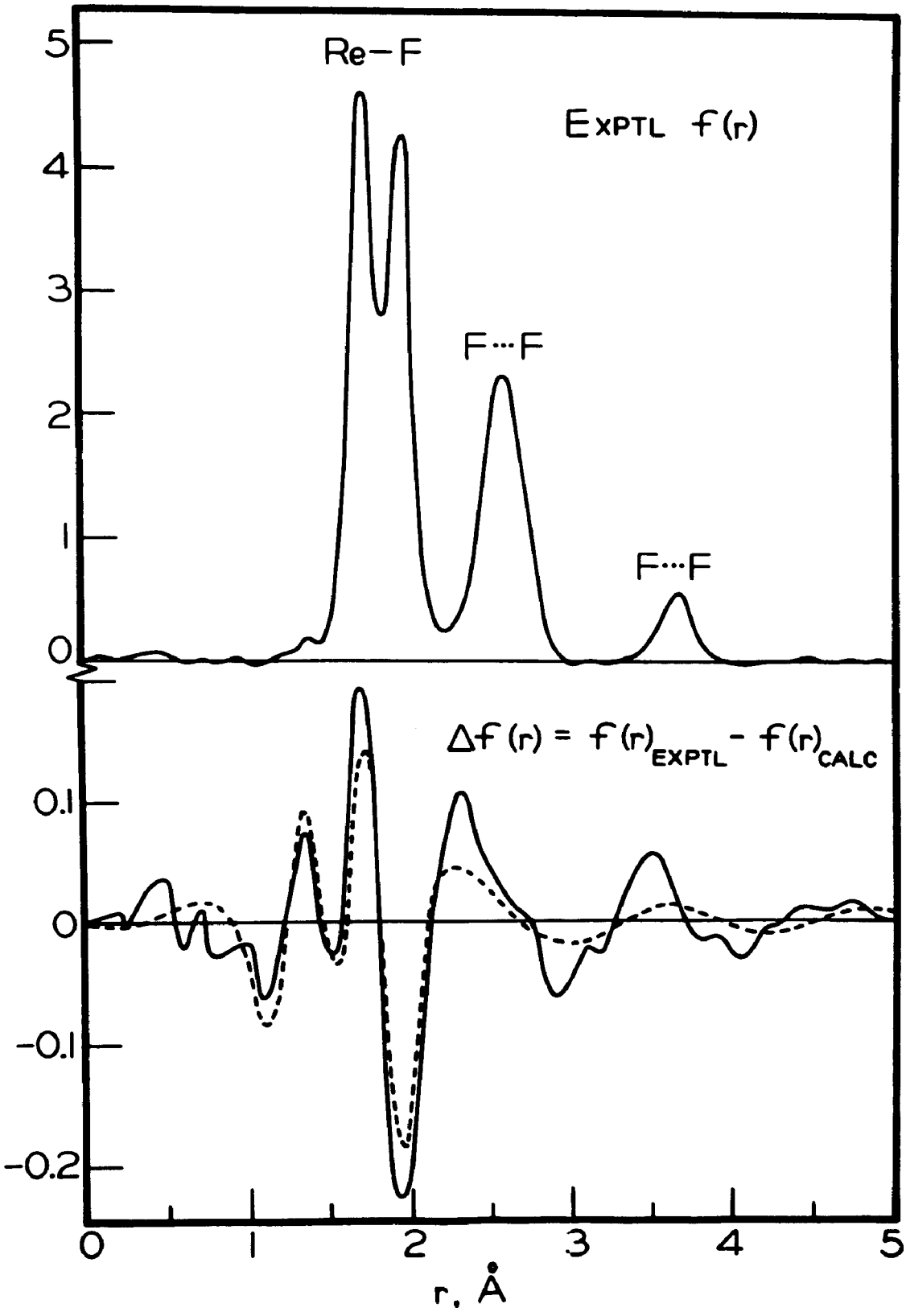

Re–F
Exptl f(r)
F···F
F···F
Δf(r) = f(r)EXPTL - f(r)CALC
5
4
3
2
1
0
0.1
0
-0.1
-0.2
0
1
2
3
4
5
r, Å

Figure 4 Molecular intensity curves for $ReF_6$. The dashed curve is the difference curve which was obtained by Jacob and Bartell.

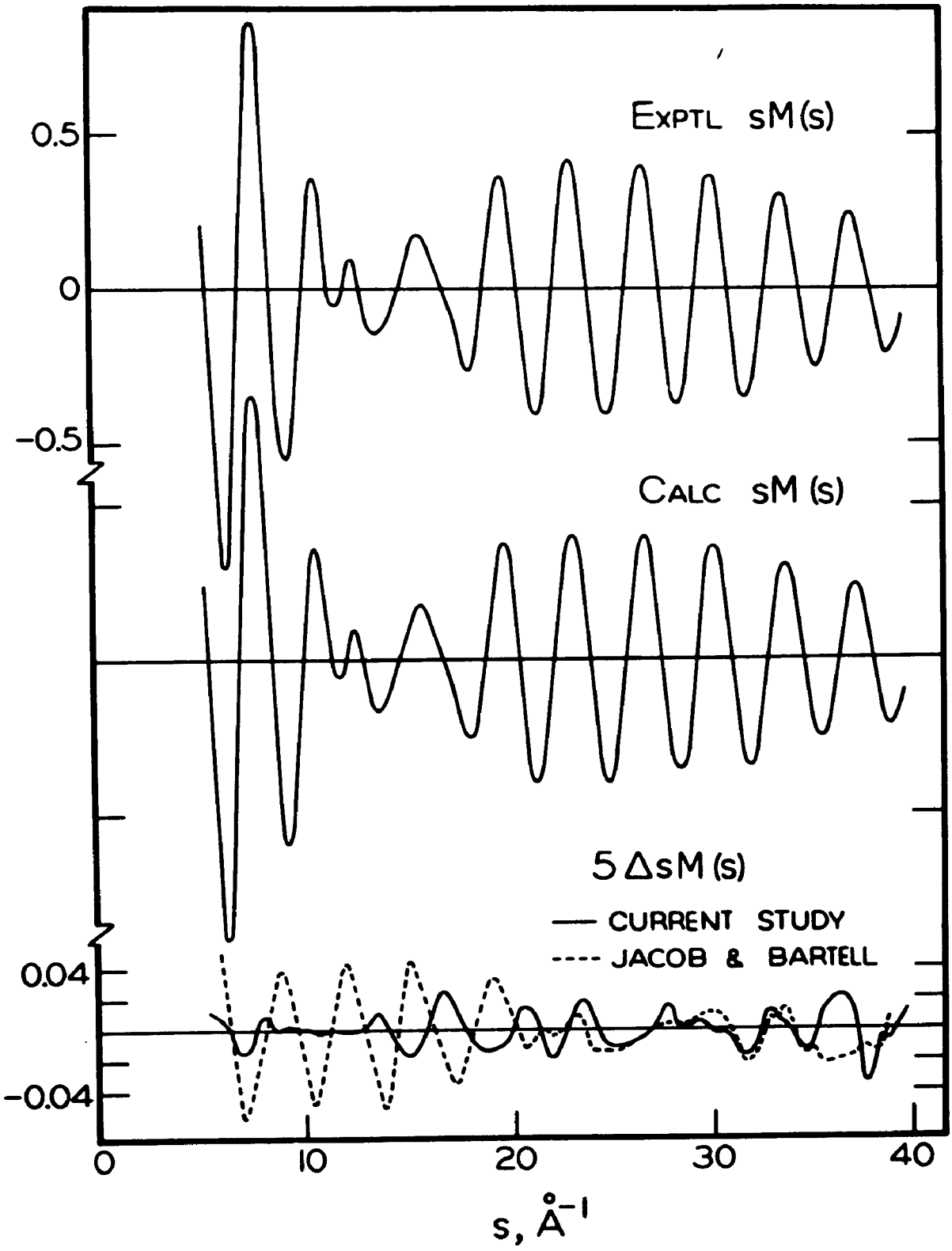

EXPTL sM(s)
CALC sM (s)
5 ΔsM (s)
CURRENT STUDY
JACOB & BARTELL
0.5
0
-0.5
0.04
-0.04
0
10
20
30
40
s, Å⁻¹

TABLE 3

A. COMPARISON OF MOLECULAR PARAMETERS FOR $ReF_6$

| | Current[a] | Previous | Spectroscopic[f] |
|---|---|---|---|
| $r_g$(Re-F), Å | 1.830(6)[c] | 1.832 | - |
| $l_g$(Re-F), Å | 0.043(5) | 0.043 | 0.039 |
| $l_g$(F-F), Å | 0.098(20) | 0.116 | 0.092 |
| $l_g$(F--F), Å | 0.058(8) | 0.072 | 0.052 |
| $\sigma(I_o)/\bar{I}_o$[b] | 0.00048 | 0.00116 | |

B. CORRELATION COEFFICIENTS FOR $ReF_6$[d]

| | $r_g$(Re-F) | $l_g$(Re-F) | $l_g$(F-F) | $l_g$(F--F) | R |
|---|---|---|---|---|---|
| $r_g$(Re-F) | 1 | -0.04 | 0.00 | 0.02 | -0.01 |
| $l_g$(Re-F) | | 1 | 0.37 | 0.13 | 0.69 |
| $l_g$(F-F) | | | 1 | 0.09 | 0.53 |
| $l_g$(F--F) | | | | 1 | 0.17 |
| R[e] | | | | | 1 |

a) The shrinkages used for the long and short F-F distances were .007 Å and .002 Å respectively.

b) The intensity data were weighted proportional to $s^2$.

c) All estimated uncertainties include random and systematic errors and correspond to $2.5\sigma$ where $\sigma$ is the standard deviation. Systematic errors for wavelength and camera distance measurement and radial measurement in microphotometering are estimated to be 3, 3, and 2 parts per 10,000.

d) Matrix elements are given by

$$\rho_{ij} = (M_x^w)_{ij} / [(M_x^w)_{ii}(M_x^w)_{jj}]^{\frac{1}{2}}$$

where $M_x^w$ is the error matrix. Elements less than 0.01 are

TABLE 3 (continued)

assigned a value equal to zero.

e) Index of resolution; dimensionless and in the current work equal to 1.07 and 1.09 for the long and short camera distances respectively.

f) See reference 14.

Figure 5 Fourier sine transform of the calculated multiple scattering contribution to the reduced molecular intensity function for $XeOF_4$ (solid line) and the residual of the radial distribution function obtained by Jacob and Bartell.

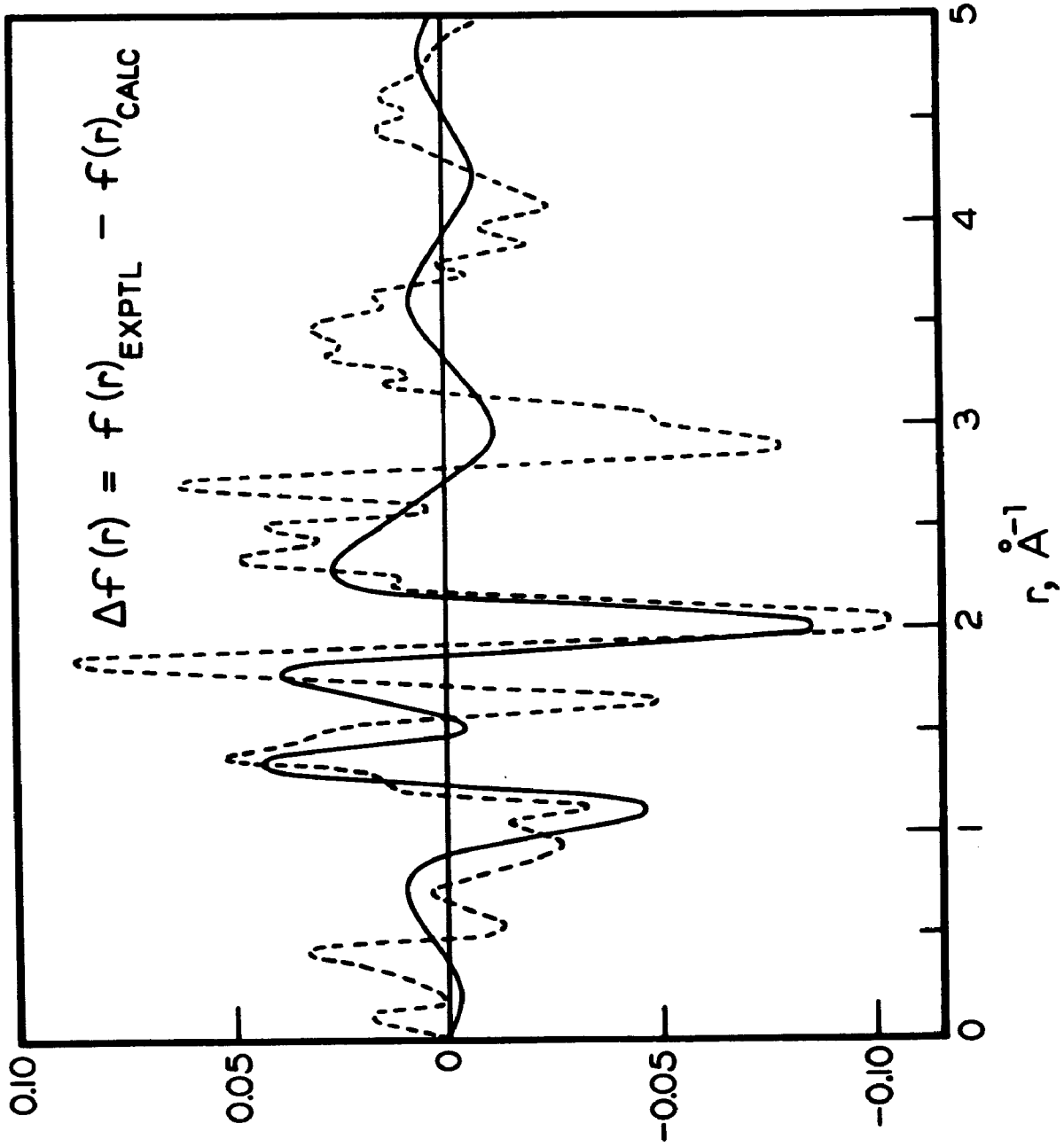

$\Delta f(r) = f(r)_{EXPTL} - f(r)_{CALC}$
0.10
0.05
0
-0.05
-0.10
0
1
2
3
4
5
r, Å$^{-1}$

Figure 6 Molecular intensity curves for $XeOF_4$. The dashed curve is the difference curve which was obtained by Jacob and Bartell.

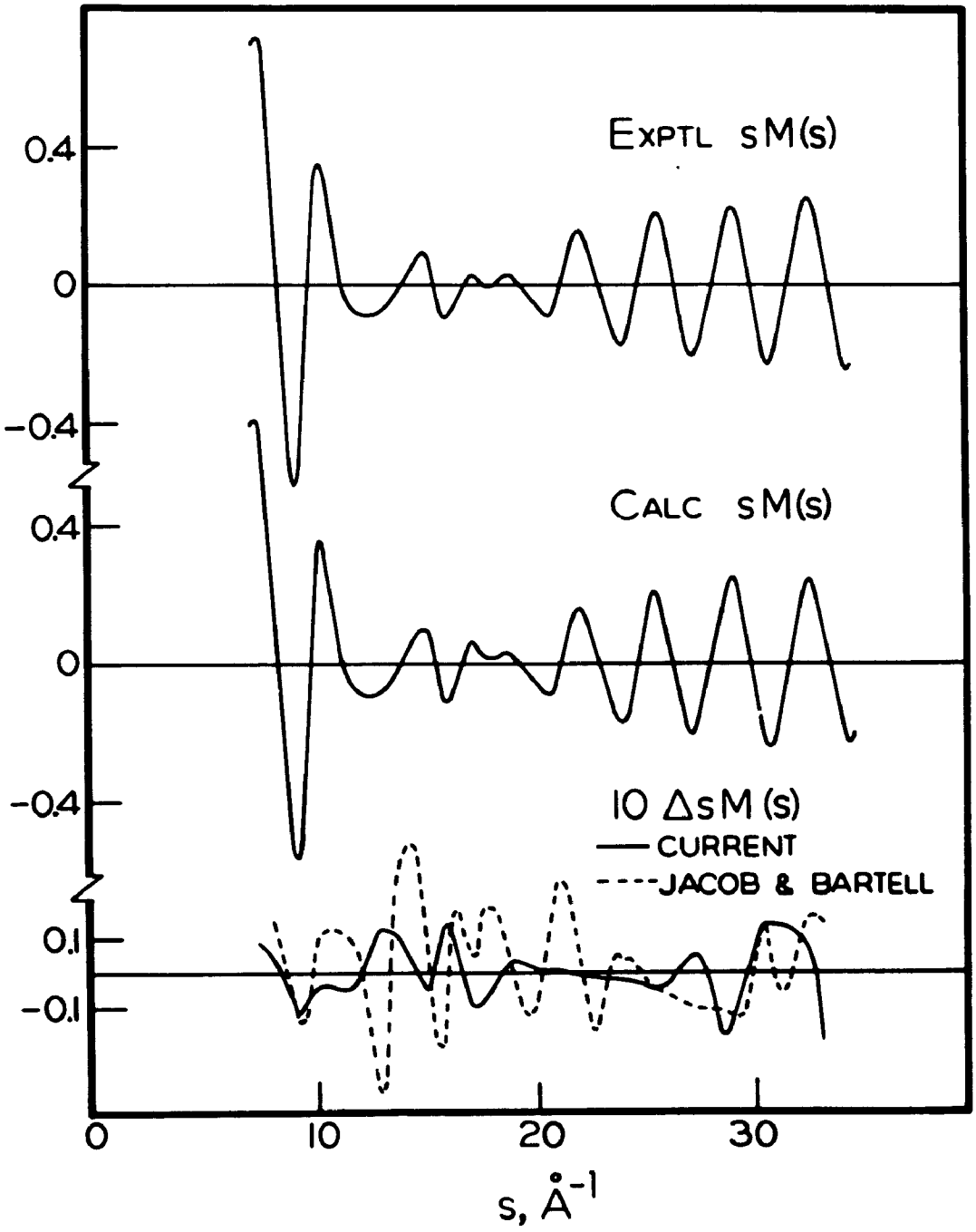

EXPTL sM(s)
CALC sM(s)
10 ΔsM(s)
CURRENT
JACOB & BARTELL
0.4
0
-0.4
0.4
0
-0.4
0.1
-0.1
0
10
20
30
s, Å-1

TABLE 4

A. COMPARISON OF MOLECULAR PARAMETERS FOR $XeOF_4$

| | Current[a] | Previous[c] | Spectroscopic[g] |
|---|---|---|---|
| $r_g$(Xe-O), Å | 1.696(6)[d] | 1.711 | 1.706 |
| $r_g$(Xe-F), Å | 1.904(4) | 1.901 | 1.903 |
| ∠O-Xe-F | 92.45°(70) | 91.93° | 91.8° |
| $l_g$(Xe-O), Å | 0.034(4) | 0.036 | 0.036 |
| $l_g$(Xe-F), Å | 0.045(3) | 0.048 | 0.045 |
| $l_g$(O-F), Å | 0.080(6) | 0.074 | 0.080 |
| $l_g$(F-F), Å | 0.124(10) | 0.136 | 0.120 |
| $l_g$(F--F), Å | 0.065(13) | 0.067 | 0.061 |
| $\sigma(I_o)/\bar{I}_o$[b] | 0.00039 | 0.00074 | |

a) Shrinkages for the O-F distance and the long and short F-F distances were 0.002 Å, 0.007 Å and 0.001 Å respectively.

b) Sigma of intensity based on $s^2$ weighting.

c) This is Jacob and Bartell's results for the analysis of the electron diffraction data alone.

d) All estimated uncertainties include random and systematic errors and correspond to $2.5\sigma$ where $\sigma$ is the standard deviation. Systematic errors for wavelength and camera distance measurements and radial measurement in microphotometering are estimated to be 3, 3 and 2 parts per 10,000.

TABLE 4 (continued)

B. CORRELATION COEFFICIENTS FOR $XeOF_4$[e]

| | $r_g$(Xe-F) | $r_g$(Xe-O) | ∠O-Xe-F | $l_g$(Xe-O) | $l_g$(Xe-F) | $l_g$(O-F) | $l_g$(F-F) | $l_g$(F--F) | R |
|---|---|---|---|---|---|---|---|---|---|
| $r_g$(Xe-O) | 1 | -0.57 | -0.07 | -0.07 | 0.15 | 0.00 | 0.09 | 0.00 | 0.06 |
| $r_g$(Xe-F) | | 1 | -0.05 | -0.17 | 0.18 | -0.07 | 0.00 | 0.01 | -0.02 |
| ∠O-Xe-F | | | 1 | 0.01 | -0.15 | -0.43 | 0.70 | 0.00 | -0.30 |
| $l_g$(Xe-O) | | | | 1 | -0.58 | 0.05 | -0.03 | 0.03 | 0.00 |
| $l_g$(Xe-F) | | | | | 1 | 0.14 | 0.05 | 0.03 | 0.57 |
| $l_g$(O-F) | | | | | | 1 | -0.50 | 0.02 | 0.32 |
| $l_g$(F-F) | | | | | | | 1 | 0.02 | 0.00 |
| $l_g$(F--F) | | | | | | | | 1 | 0.08 |
| R[f] | | | | | | | | | 1 |

e) Matrix elements are given by

$$\rho_{ij} = (M_x^w)_{ij} / [(M_x^w)_{ii}(M_x^w)_{jj}]^{\frac{1}{2}}$$

where $M_x^w$ is the bona fide error matrix.

f) Index of resolution; dimensionless and in the present work equal to .99 and .99 for the long and short camera distances respectively.

g) See reference 23. The spectroscopic r values have been augmented by 0.003 Å in order to put them of an $r_g$ basis.

TABLE 5

21 cm Camera Distance Intensity Data For $Pt(PF_3)_4$ ($R^3$ Sector)

| s | $I_o(s)$ | $I_B(s)$ | s | $I_o(s)$ | $I_B(s)$ | s | $I_o(s)$ | $I_B(s)$ | s | $I_o(s)$ | $I_B(s)$ |
|---|---|---|---|---|---|---|---|---|---|---|---|
| 3.217 | 1.8855 | | 7.657 | 1.9525 | 2.1831 | 12.067 | 2.1813 | 2.1602 | 16.429 | 2.1973 | 2.1676 |
| 3.340 | 1.9496 | | 7.780 | 2.0124 | 2.1820 | 12.189 | 2.1848 | 2.1600 | 16.549 | 2.2101 | 2.1682 |
| 3.464 | 2.0393 | | 7.903 | 2.0790 | 2.1809 | 12.311 | 2.1873 | 2.1599 | 16.669 | 2.2192 | 2.1687 |
| 3.588 | 2.1546 | | 8.026 | 2.1446 | 2.1798 | 12.433 | 2.1882 | 2.1598 | 16.790 | 2.2244 | 2.1693 |
| 3.711 | 2.2628 | | 8.149 | 2.2051 | 2.1788 | 12.554 | 2.1883 | 2.1597 | 16.910 | 2.2270 | 2.1699 |
| 3.835 | 2.4193 | | 8.272 | 2.2531 | 2.1778 | 12.676 | 2.1884 | 2.1596 | 17.030 | 2.2264 | 2.1705 |
| 3.958 | 2.5235 | | 8.395 | 2.2885 | 2.1768 | 12.798 | 2.1884 | 2.1596 | 17.150 | 2.2232 | 2.1711 |
| 4.082 | 2.5814 | | 8.518 | 2.3152 | 2.1758 | 12.920 | 2.1894 | 2.1596 | 17.270 | 2.2171 | 2.1718 |
| 4.205 | 2.5659 | | 8.641 | 2.3294 | 2.1749 | 13.041 | 2.1884 | 2.1596 | 17.390 | 2.2097 | 2.1724 |
| 4.329 | 2.4956 | | 8.763 | 2.3389 | 2.1740 | 13.163 | 2.1897 | 2.1596 | 17.510 | 2.2010 | 2.1731 |
| 4.452 | 2.3574 | | 8.886 | 2.3419 | 2.1732 | 13.284 | 2.1919 | 2.1596 | 17.630 | 2.1942 | 2.1738 |
| 4.576 | 2.2183 | | 9.009 | 2.3421 | 2.1723 | 13.406 | 2.1931 | 2.1597 | 17.749 | 2.1867 | 2.1745 |
| 4.699 | 2.0928 | | 9.132 | 2.3353 | 2.1715 | 13.527 | 2.1940 | 2.1598 | 17.869 | 2.1802 | 2.1752 |
| 4.823 | 2.0107 | | 9.256 | 2.3192 | 2.1707 | 13.649 | 2.1935 | 2.1599 | 17.989 | 2.1756 | 2.1759 |
| 4.946 | 1.9931 | | 9.377 | 2.2983 | 2.1700 | 13.770 | 2.1953 | 2.1600 | 18.108 | 2.1718 | 2.1766 |
| 5.070 | 2.0343 | | 9.500 | 2.2694 | 2.1693 | 13.891 | 2.1948 | 2.1601 | 18.228 | 2.1693 | 2.1774 |
| 5.193 | 2.1194 | | 9.622 | 2.2368 | 2.1686 | 14.013 | 2.1913 | 2.1603 | 18.348 | 2.1691 | 2.1782 |
| 5.316 | 2.2300 | | 9.745 | 2.2034 | 2.1679 | 14.134 | 2.1863 | 2.1605 | 18.467 | 2.1684 | 2.1789 |
| 5.440 | 2.3224 | | 9.867 | 2.1740 | 2.1673 | 14.255 | 2.1781 | 2.1607 | 18.586 | 2.1678 | 2.1797 |
| 5.563 | 2.3877 | | 9.990 | 2.1488 | 2.1667 | 14.376 | 2.1675 | 2.1609 | 18.706 | 2.1684 | 2.1805 |
| 5.687 | 2.4412 | | 10.112 | 2.1274 | 2.1661 | 14.497 | 2.1558 | 2.1612 | 18.825 | 2.1664 | 2.1814 |
| 5.810 | 2.4636 | | 10.235 | 2.1102 | 2.1655 | 14.618 | 2.1419 | 2.1614 | 18.944 | 2.1660 | 2.1822 |
| 5.933 | 2.4730 | | 10.357 | 2.0957 | 2.1650 | 14.739 | 2.1297 | 2.1617 | 19.064 | 2.1639 | 2.1830 |
| 6.056 | 2.4647 | | 10.479 | 2.0826 | 2.1645 | 14.860 | 2.1202 | 2.1620 | 19.183 | 2.1622 | 2.1839 |
| 6.180 | 2.4436 | | 10.602 | 2.0721 | 2.1640 | 14.981 | 2.1102 | 2.1624 | 19.302 | 2.1590 | 2.1847 |
| 6.303 | 2.4064 | | 10.724 | 2.0665 | 2.1635 | 15.102 | 2.1034 | 2.1627 | 19.421 | 2.1584 | 2.1856 |
| 6.426 | 2.3489 | | 10.846 | 2.0636 | 2.1631 | 15.223 | 2.1002 | 2.1631 | 19.540 | 2.1573 | 2.1865 |
| 6.549 | 2.2746 | 2.1947 | 10.969 | 2.0662 | 2.1627 | 15.344 | 2.0988 | 2.1634 | 19.659 | 2.1574 | 2.1874 |
| 6.673 | 2.1827 | 2.1933 | 11.091 | 2.0757 | 2.1623 | 15.465 | 2.1001 | 2.1638 | 19.778 | 2.1584 | 2.1883 |
| 6.796 | 2.0882 | 2.1919 | 11.213 | 2.0887 | 2.1620 | 15.585 | 2.1051 | 2.1642 | 19.896 | 2.1617 | 2.1892 |
| 6.919 | 1.9980 | 2.1906 | 11.335 | 2.1055 | 2.1617 | 15.706 | 2.1131 | 2.1647 | 20.015 | 2.1671 | 2.1902 |
| 7.042 | 1.9281 | 2.1892 | 11.457 | 2.1227 | 2.1614 | 15.827 | 2.1233 | 2.1651 | 20.134 | 2.1735 | 2.1911 |
| 7.165 | 1.8792 | 2.1879 | 11.579 | 2.1390 | 2.1611 | 15.947 | 2.1369 | 2.1656 | 20.252 | 2.1805 | 2.1921 |
| 7.288 | 1.8614 | 2.1867 | 11.701 | 2.1538 | 2.1608 | 16.068 | 2.1518 | 2.1661 | 20.371 | 2.1894 | 2.1930 |
| 7.411 | 1.8697 | 2.1855 | 11.823 | 2.1655 | 2.1606 | 16.188 | 2.1672 | 2.1666 | 20.489 | 2.1960 | |
| 7.534 | 1.8999 | 2.1843 | 11.945 | 2.1740 | 2.1604 | 16.308 | 2.1831 | 2.1671 | 20.608 | 2.2022 | |

11 cm Camera Distance Intensity Data For $Pt(PF_3)_4$ ($R^3$ Sector)

| s | $I_o(s)$ | $I_B(s)$ | s | $I_o(s)$ | $I_B(s)$ | s | $I_o(s)$ | $I_B(s)$ | s | $I_o(s)$ | $I_B(s)$ |
|---|---|---|---|---|---|---|---|---|---|---|---|
| 8.487 | 6.1150 | | 16.849 | 5.9059 | 5.7713 | 24.972 | 5.8747 | 5.8023 | 32.762 | 5.8822 | 5.8589 |
| 8.722 | 6.1848 | | 17.078 | 5.9010 | 5.7717 | 25.194 | 5.8578 | 5.8036 | 32.973 | 5.8920 | 5.8607 |
| 8.956 | 6.2338 | | 17.307 | 5.8766 | 5.7721 | 25.415 | 5.8432 | 5.8049 | 33.183 | 5.8980 | 5.8625 |
| 9.190 | 6.2189 | | 17.536 | 5.8387 | 5.7726 | 25.635 | 5.8280 | 5.8062 | 33.393 | 5.8988 | 5.8644 |
| 9.424 | 6.1188 | | 17.765 | 5.7998 | 5.7731 | 25.856 | 5.8096 | 5.8076 | 33.603 | 5.8937 | 5.8662 |
| 9.658 | 5.9573 | | 17.994 | 5.7656 | 5.7736 | 26.076 | 5.8005 | 5.8089 | 33.813 | 5.8840 | 5.8681 |
| 9.892 | 5.8013 | | 18.222 | 5.7488 | 5.7742 | 26.296 | 5.7954 | 5.8103 | 34.022 | 5.8722 | 5.8700 |
| 10.126 | 5.6843 | | 18.450 | 5.7401 | 5.7747 | 26.516 | 5.7921 | 5.8117 | 34.231 | 5.8652 | 5.8719 |
| 10.360 | 5.6174 | | 18.678 | 5.7384 | 5.7754 | 26.735 | 5.7929 | 5.8131 | 34.439 | 5.8565 | 5.8738 |
| 10.594 | 5.5548 | | 19.134 | 5.7236 | 5.7766 | 26.954 | 5.7954 | 5.8145 | 34.648 | 5.8535 | 5.8757 |
| 10.827 | 5.5138 | | 19.361 | 5.7147 | 5.7773 | 27.173 | 5.7978 | 5.8160 | 34.856 | 5.8535 | 5.8776 |
| 11.061 | 5.5413 | | 19.588 | 5.7063 | 5.7781 | 27.392 | 5.8057 | 5.8175 | 35.063 | 5.8546 | 5.8795 |
| 11.294 | 5.6181 | 5.7690 | 19.815 | 5.7135 | 5.7788 | 27.610 | 5.8078 | 5.8189 | 35.271 | 5.8613 | 5.8814 |
| 11.527 | 5.7093 | 5.7689 | 20.042 | 5.7335 | 5.7796 | 27.828 | 5.8164 | 5.8204 | 35.478 | 5.8643 | 5.8834 |
| 11.760 | 5.7829 | 5.7687 | 20.269 | 5.7608 | 5.7803 | 28.046 | 5.8151 | 5.8219 | 35.684 | 5.8776 | 5.8853 |
| 11.993 | 5.8299 | 5.7686 | 20.495 | 5.7901 | 5.7812 | 28.263 | 5.8169 | 5.8235 | 35.890 | 5.8818 | 5.8873 |
| 12.226 | 5.8520 | 5.7685 | 20.721 | 5.8204 | 5.7820 | 28.480 | 5.8186 | 5.8250 | 36.096 | 5.8898 | 5.8893 |
| 12.458 | 5.8513 | 5.7684 | 20.947 | 5.8381 | 5.7829 | 28.697 | 5.8207 | 5.8266 | 36.302 | 5.8905 | 5.8912 |
| 12.691 | 5.8497 | 5.7683 | 21.173 | 5.8514 | 5.7838 | 28.914 | 5.8261 | 5.8282 | 36.507 | 5.8921 | 5.8932 |
| 12.923 | 5.8388 | 5.7683 | 21.398 | 5.8591 | 5.7847 | 29.130 | 5.8353 | 5.8297 | 36.712 | 5.8914 | 5.8952 |
| 13.155 | 5.8410 | 5.7683 | 21.623 | 5.8629 | 5.7856 | 29.346 | 5.8459 | 5.8314 | 36.917 | 5.8917 | 5.8972 |
| 13.387 | 5.8448 | 5.7683 | 21.848 | 5.8610 | 5.7866 | 29.562 | 5.8602 | 5.8330 | 37.121 | 5.8940 | 5.8992 |
| 13.619 | 5.8524 | 5.7683 | 22.073 | 5.8494 | 5.7876 | 29.777 | 5.8727 | 5.8346 | 37.325 | 5.8927 | 5.9012 |
| 13.851 | 5.8491 | 5.7683 | 22.297 | 5.8308 | 5.7886 | 29.993 | 5.8770 | 5.8363 | 37.529 | 5.8960 | 5.9032 |
| 14.083 | 5.8288 | 5.7684 | 22.522 | 5.7956 | 5.7896 | 30.207 | 5.8794 | 5.8379 | 37.732 | 5.9044 | 5.9052 |
| 14.314 | 5.7846 | 5.7685 | 22.746 | 5.7606 | 5.7906 | 30.422 | 5.8698 | 5.8396 | 37.935 | 5.9147 | 5.9073 |
| 14.545 | 5.7231 | 5.7686 | 22.969 | 5.7227 | 5.7917 | 30.636 | 5.8547 | 5.8413 | 38.138 | 5.9211 | 5.9093 |
| 14.776 | 5.6599 | 5.7688 | 23.193 | 5.6988 | 5.7928 | 30.850 | 5.8336 | 5.8430 | 38.340 | 5.9307 | 5.9113 |
| 15.007 | 5.6099 | 5.7689 | 23.416 | 5.6932 | 5.7939 | 31.064 | 5.8189 | 5.8447 | 38.542 | 5.9296 | 5.9134 |
| 15.238 | 5.5796 | 5.7691 | 23.639 | 5.7114 | 5.7951 | 31.277 | 5.8096 | 5.8464 | 38.743 | 5.9269 | 5.9154 |
| 15.469 | 5.5798 | 5.7694 | 23.862 | 5.7431 | 5.7962 | 31.490 | 5.8025 | 5.8482 | 38.944 | 5.9271 | 5.9175 |
| 15.699 | 5.6084 | 5.7696 | 24.085 | 5.7895 | 5.7974 | 31.703 | 5.8061 | 5.8499 | 39.145 | 5.9269 | 6.2984 |
| 15.930 | 5.6650 | 5.7699 | 24.307 | 5.8296 | 5.7986 | 31.915 | 5.8177 | 5.8517 | 39.346 | 5.9279 | |
| 16.160 | 5.7412 | 5.7702 | 24.529 | 5.8606 | 5.7998 | 32.127 | 5.8322 | 5.8535 | | | |
| 16.390 | 5.8168 | 5.7705 | 24.751 | 5.8757 | 5.8011 | 32.339 | 5.8484 | 5.8553 | | | |
| 16.619 | 5.8758 | 5.7709 | 24.972 | 5.8747 | 5.8023 | 32.551 | 5.8685 | 5.8571 | | | |

Figure 7 Molecular intensity curves for $Pt(PF_3)_4$. The dashed curve is the difference curve obtained from an analysis of the intensity data for which no multiple scattering corrections were applied.

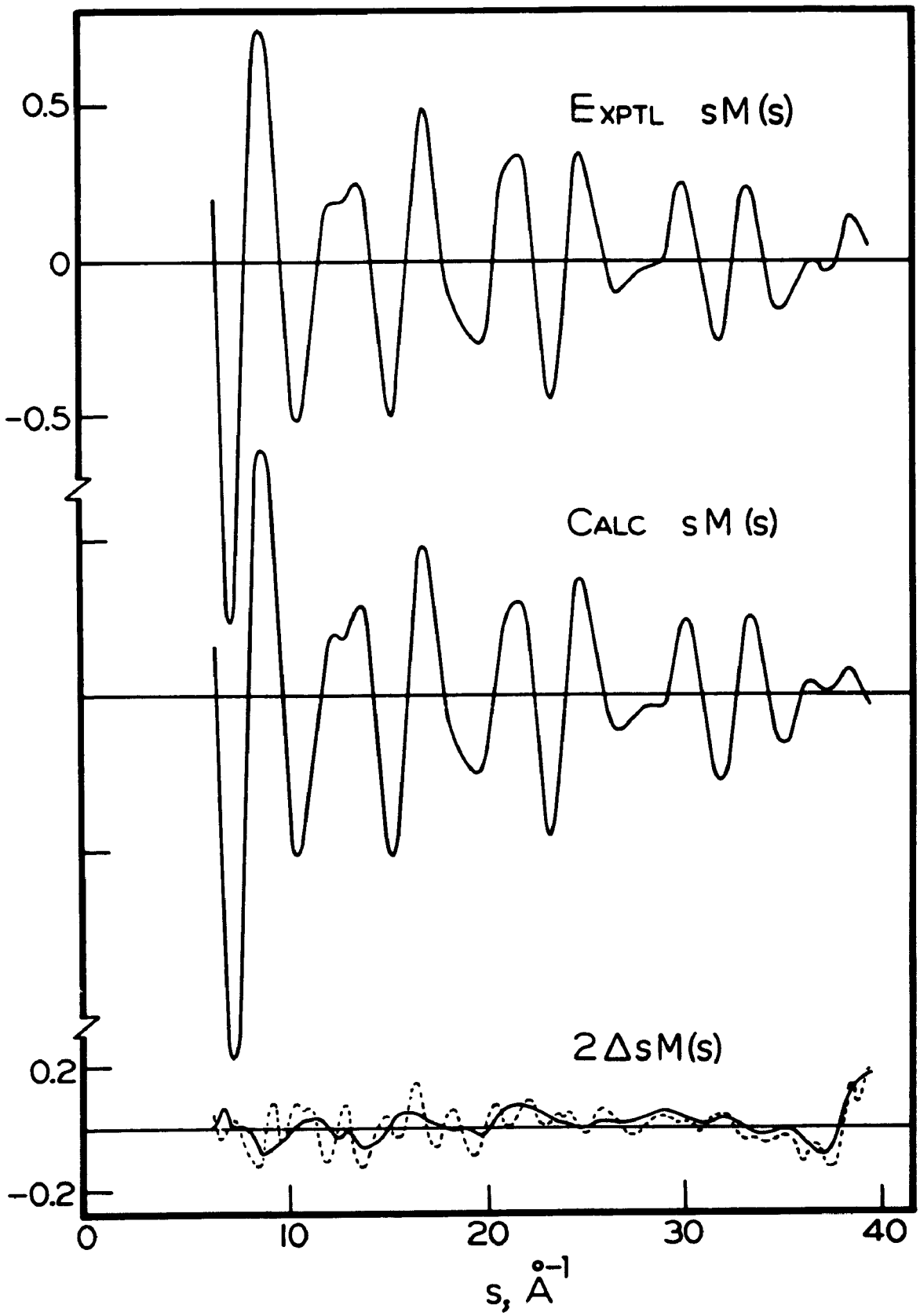

0.5
0
-0.5
EXPTL sM(s)
CALC sM(s)
2ΔsM(s)
0.2
-0.2
0
10
20
30
40
s, Å$^{-1}$

TABLE 6

A. MOLECULAR PARAMETERS FOR $Pt(PF_3)_4$

| | I[a] | II[b] |
|---|---|---|
| $r_g$(Pt-P), Å | 2.229(5)[g] | 2.229(6) |
| $r_g$(P-F), Å | 1.550(4) | 1.551(4) |
| ∠Pt-P-F | 118.9°(4) | 118.9°(4) |
| $l_g$(Pt-P), Å | 0.050(3) | 0.050(3) |
| $l_g$(P-F), Å | 0.042(3) | 0.042(3) |
| $l_g$(F--F), Å[c] | 0.070(8) | 0.065(8) |
| $l_g$(Pt--F), Å | 0.089(8) | 0.089(8) |
| $l_g$(P--P), Å | 0.123(17) | 0.105(20) |
| $l_g$(P--F), Å[d] | 0.186(50) | 0.163(45) |
| $l_g$(F---F), Å[d,f] | 0.2 | 0.2 |
| $\sigma(I_o)/\bar{I}_o$[e] | 0.0010 | 0.0012 |

a) Three atom corrections applied.

b) No multiple scattering corrections applied.

c) Fluorine atoms are on same phosphorous atom.

d) This parameter is rotation dependent.

e) Sigma based on $s^2$ weighting of intensity.

f) Parameter was not refined.

g) All estimated uncertainties include random and systematic errors and correspond to $2.5\sigma$ where $\sigma$ is the standard deviation. Systematic errors for wavelength and camera distance measurement and radial measurement in microphotometering are estimated to be 3, 3 and 2 parts per ten thousand respectively.

TABLE 6 (continued)

B. CORRELATION COEFFICIENTS FOR $Pt(PF_3)_4$[h]

| | $r_g$(P-F) | ∢Pt-P-F | $l_g$(Pt-P) | $l_g$(P-F) | $l_g$(F--F) | $l_g$(Pt--F) | $l_g$(P--P) | $l_g$(P--F) | R |
|---|---|---|---|---|---|---|---|---|---|
| $r_g$(Pt-P) | -0.18 | -0.81 | -0.08 | 0.27 | 0.34 | 0.16 | 0.00 | -0.05 | 0.41 |
| $r_g$(P-F) | 1 | -0.18 | 0.00 | -0.08 | -0.11 | -0.03 | -0.02 | -0.01 | -0.11 |
| ∢Pt-P-F | | 1 | -0.06 | -0.38 | -0.21 | -0.15 | -0.02 | -0.15 | -0.57 |
| $l_g$(Pt-P) | | | 1 | 0.26 | -0.31 | 0.03 | 0.00 | 0.14 | 0.28 |
| $l_g$(P-F) | | | | 1 | 0.23 | 0.14 | 0.00 | 0.22 | 0.73 |
| $l_g$(F--F) | | | | | 1 | 0.12 | 0.00 | -0.04 | 0.33 |
| $l_g$(Pt--F) | | | | | | 1 | 0.26 | -0.03 | 0.20 |
| $l_g$(P--P) | | | | | | | 1 | 0.24 | 0.00 |
| $l_g$(P--F) | | | | | | | | 1 | 0.30 |
| $R^i$ | | | | | | | | | 1 |

h) Matrix elements are given by

$$\rho_{ij} = (M_x^w)_{ij} / [(M_x^w)_{ii}(M_x^w)_{jj}]^{\frac{1}{2}}$$

where $M_x^w$ is the bona fide error matrix.

i) Index of resolution; dimensionless. and in the present work equal to .90 and .86 for the long and short camera distances respectively.

## REFERENCES

### PART I


1. L. S. Bartell, K. Kuchitsu and R. J. De Neui, J. Chem. Phys., 35, 1211(1961).
2. T. L. Boates, Doctoral Dissertation, Iowa State University, 1966.
3. L. S. Bartell, in 'Physical Methods of Chemistry'(A. Weissberger and B. W. Rossiter, ed.), Part III D, Interscience, New York, 1972, p. 133.
4. Ibid., p. 134.
5. R. A. Bonham and H. L. Cox, Jr., J. Chem. Phys., 47, 2599(1967); International Tables of X-Ray Crystallography, Kynoch Press, Birmingham, England, 1952; R. F. Pohler and H. P. Hanson, J. Chem. Phys., 42, 2347(1965); C. Tavard, D. Nicholas and M. Rouault, J. Chem. Phys., 64, 540(1967); L. Schafer, A. C. Yates and R. A. Bonham, J. Chem. Phys., 55, 3055(1971).
6. L. S. Bartell, Op. Cit., p. 133.
7. T. C. Wong and L. S. Bartell, J. Chem. Phys., 58, 5654(1973).
8. L. S. Bartell, Op. Cit., p. 136.
9. K. Kuchitsu and L. S. Bartell, J. Chem. Phys., 35, 1945(1961).
10. L. S. Bartell, Op. Cit..
11. T. L. Boates, Op. Cit..
12. L. Schafer, A. C. Yates and R. A. Bonham, Op. Cit..

13. C. H. Townes, F. R. Merritt and B. D. Wright, Phys. Rev., 73, 1334(1948).

14. S. J. Cyvin, 'Vibrations and Mean Square Amplitudes of Vibration', Elsvier, Amsterdam, 1968, p. 240.

15. E. J. Jacob and L. S. Bartell, J. Chem. Phys., 56, 2231(1970).

16. L. S. Bartell and T. C. Wong, J. Chem. Phys., 57, 2364(1972).

17. R. A. Bonham and T. Ukaji, J. Chem. Phys., 36, 72(1962).

18. W. Heisenberg, Physik. Z., 32, 737(1931); L. Bewilogua, Ibid., 32, 740(1931).

19. H. L. Cox, Jr., Doctoral Dissertation, Indiana University, 1967.

20. L. Schafer, A. C. Yates and R. A. Bonham, Op. Cit..

21. E. J. Jacob, H. B. Thompson and L. S. Bartell, J. Mol. Struc., 8, 383(1971).

22. L. Schafer, A. C. Yates and R. A. Bonham, Op. Cit..

23. J. F. Martins and E. B. Wilson, Jr., J. Mol. Spectry., 26, 410(1968); S. J. Cyvin, J. Brunvoll and A. G. Robiette, J. Mol. Struc., 3, 259(1969).

24. L. S. Bartell, Op. Cit..

25. T. L. Boates, Op. Cit..

26. A. Almenningen, B. Andersen and E. E. Astrup, Acta Chem. Scand., 24, 1579(1970).

27. J. C. Marriott, J. A. Salthouse and M. J. Ware, J. Chem. Commun., 595(1970).

28. G. Herzberg, 'Spectra of Diatomic Molecules', Second

Edition, D. Van Nostrand Company, Princeton, 1950, p. 542.

# Part II

## ELECTRON WAVE HOLOGRAPHY

## INTRODUCTION

In 1948, Gabor presented the idea for a new kind of microscope.[1] He showed how, in principle, to devise a two-stage holographic microscope which would be capable of extremely high magnification. In the first stage of this microscope, electron beams would be used rather than light beams to record information about the subject being viewed. In contrast to ordinary microscopy, no objective lens would be needed. The amplitude and phase of the wave from the subject (the subject wave) would be established by superposing the wave from the subject upon a wave which had not interacted with the subject (the reference wave). In the simplest variant of a holographic microscope, the sum of these waves would be recorded on a photographic emulsion. A photographic record of the intensity pattern in the wavefront is called a hologram.

The second stage would involve reconstruction of the original subject by passing light waves through the hologram. The magnification realized by such an instrument would be proportional to the ratio of the wavelength employed in the second stage to that in the first. Since electron waves envisioned for use in the first stage of the apparatus would have a wavelength only hundredths of an angstrom and light waves employed in the reconstruction

would have a wavelength of the order of thousands of angstroms, magnification could easily reach into the hundreds of thousands, exclusive of other optical factors.

The idea of using electron waves to produce a hologram has never been developed with complete success although several attempts to take advantage of Gabor's suggestion have been published.[2] One problem impeding progress in electron-wave holography is the impossibility of devising an electron laser. It is not a simple matter with electron waves to establish with arbitrary flexibility a reference wave coherent with the waves emanating from the subject to be studied. The coherence condition requires that in the first stage of the microscope the reference wave and the subject wave must have the same wavelength and a fixed phase relation during the recording of the hologram. It is well known that light beams can be generated with enormous numbers of photons exhibiting an extremely high degree of coherence and that these beams can be easily split into reference beams and beams to illuminate the subject. Thus in past years, attention has switched to a type of holography which almost exclusively utilizes lasers.

By using Gabor's original idea, a simple method for obtaining holograms of monoatomic gaseous atoms was developed. In essence, the strong scattering of electron waves by each nucleus generates a divergent reference beam which is coherent with the electron waves (the subject waves) scattered by the planetary electrons in the electron cloud

surrounding the nucleus. That is, each atom produces its own reference wave as well as subject wave, and each atom produces a wavefront at the plane of the hologram that is the same as the wavefront from every other identical atom. Figure 8 shows the reconstructed images of argon and neon. The overall magnification is roughly 500 million with a resolving power of .08 Å.

In order to lessen the possibility of confusion, it should be pointed out that in this experiment the atoms were moving and not stationary as are subjects in the more conventional laser holographic technique where the reference beam is also fixed. In atomic holography, each atom, as was mentioned in the previous paragraph, produces its own reference beam as well as subject wave and, therefore, the subject is stationary relative to the reference wave. Since each atom produces its own hologram, and since all of the holograms are centered on a common origin (the origin of the Frauenhoffer diffraction pattern of the atoms), all atomic images are exactly centered on top of each other in the reconstruction process. Because the images are all identical and the samples were pure monoatomic gases, the reconstruction was not degraded by this superposition.

The method used to obtain the pictures of argon and neon will be discussed in the next section. In addition, the theory of the recording and reconstruction process employed in atomic holography will be presented.

## EXPERIMENTAL PROCEDURE

The electron diffraction unit located at the University of Michigan was used as the first stage of the holographic microscope. Details of its construction have been covered elsewhere in the literature.[4] A well regulated power supply was used to generate a 40 kilovolt ($\pm$4 volts) electron beam during the course of the experiment. The beam current was measured directly by a Faraday cup located in the diffraction chamber and was found to be .56$\pm$0.01 micro-amperes.

The only major modification in the apparatus was a specially constructed 41 mm radius rotating sector whose angular opening was proportional to $s^4\sec^3\phi$ where

$$s = (4\pi/\lambda)\sin(\phi/2).$$

In this equation $\phi$ is the scattering angle and $\lambda$ is the wavelength of the electrons which in this experiment was equal to 0.0605$\pm$0.000003 $\mathring{A}$. The rationale of using a sector with such an angular opening will be brought out in the discussion of the theory.

The surface of the heart-shaped rotating sector was designed to sit 4 mm above the photographic plate which was used to record the hologram. The sector was constructed of brass and the sector opening was cut with a pantographic milling machine within a tolerance of 0.001 inch. The whole sector assembly was then mounted in a demagnetized Norma-Hoffman XLS bearing assembly.

Chamber pressure was kept between $10^{-4}$ and $10^{-5}$ mm Hg

during the whole experiment in order to lower the incidence of extraneous scattering effects. A .27 mm diameter nozzle made of platinum and located $11.021 \pm 0.002$ cm above the plane of the photographic plate was used to direct a fine jet of the monoatomic gas into the electron beam. Furthermore, all of the platinum parts of the nozzle assembly were painted with a graphite suspension which when dried formed a conducting outer layer that lowered the amount of extraneous scattering by the heavy metal parts.

The neon and argon samples were obtained from the Matheson Company. The purity, according to the manufacturer, was at least 99%. No further check was made of sample purity. During the course of the experiments, the gas samples were kept at a pressure of 40-50 mm Hg in one liter glass bulbs equipped with ground glass stopcock joints. The flow of gas to the diffraction chamber was regulated by a Monel valve located between the chamber and glass bulb. Pressure was sufficient to produce holograms of Ne after 20 seconds exposure and holograms of Ar after 30 seconds exposure.

Kodak Electron Image Plates were used to record the holograms. The procedure used for development of the holograms was that recommended by the manufacturer at 68° C.[5] This process gave holograms recording information extending over the range $5.9\ \text{Å}^{-1} \leqslant s \leqslant 40.1\ \text{Å}^{-1}$. Inside this range, where the intensity would theoretically approach zero rapidly, the slit became too narrow for accurate machining

and it was covered with a mask, accordingly.

In order to enlarge the resultant atomic image, each hologram, after development, was reduced in dimension by taking a picture of it and thereby recording a positive of the hologram's image on Polaroid Continuous Tone Slide Film. By this method, the hologram was reduced from a radius of 41 mm to one of 5mm (or reduced by a factor of 8.2). Before photographing the hologram, an opaque mask was laid over the hologram and covered the region extending beyond the 41 mm radius limit of actual data collection. This masking insured that all spurious light not associated with the hologram was prevented from interfering with the reconstruction.

Reconstructed images were obtained by placing reduced holograms in a laser diffractometer. The latter is an instrument which takes the optical transform of any pattern in its path.[6] In its basic form, the diffractometer consists of a monochromatic, point light source, a positive lens of long focal length and, in most cases, an eyepiece placed at the output of the diffractometer. Figure 9 illustrates in a schematic form the device used.

In the present case, the light source for the laser diffractometer was a He-Ne single mode laser whose continuous 1 mw output had a wavelength equal to 6328 Å. The laser was fitted with a diverging lens of focal length -8.6 mm. The positive lens was a 3 inch diameter achromat (an unnecessary property) with a focal length of 45 inches. The eyepiece

was a zoom lens which was used at the 14 mm setting. All of the optical equipment was obtained from Edmund Scientific Company.

In practice, the distance from the light source to the positive lens was set equal to the distance from the positive lens to the eyepiece, namely 7.5 feet. Photographs of the reconstructed atomic images were made using the eyepiece as a projector lens.

## DISCUSSION OF THEORY

In the development of the theoretical basis for atomic holography, an atom is assumed to have an electronic charge density $\rho(\vec{r})$ and a nuclear charge of Z at $\vec{r}$ equal to zero. The x-ray elastic scattering factor for a monoatomic sample may be written as[7]

$$F(\vec{s}) = \int \exp(i\vec{s}_1 \cdot \vec{r}_1)\rho(\vec{r}_1)d^3\vec{r}_1 \qquad (1a)$$

$$= \int \exp(i\vec{s}_1 \cdot \vec{b}_1)\rho^P(\vec{b}_1)d^2\vec{b}_1. \qquad (1b)$$

In the above equation $\vec{s}_1$ equals $(\vec{k}_o)_1 - (\vec{k}_s)_1$ where $(\vec{k}_o)_1$ and $(\vec{k}_s)_1$ are the incident and scattered wave vectors respectively in the first stage of the holographic microscope and the intergration is over the plane in which $\vec{b}_1$ ranges. The projected electron density, $\rho^P(\vec{b}_1)$, is given by the expression

$$\rho^P(\vec{b}_1) = \int_{-\infty}^{\infty} \rho(\vec{b}_1, z_1)dz_1 \qquad (2)$$

In the above equation, $\rho^P(\vec{b}_1)$ is the electron charge density summed from back to front of the atom along the direction of the vector $(\vec{k}_{os})_1$, where $\vec{b}_1$ is perpendicular to the vector $(\vec{k}_{os})_1$. The vector $(\vec{k}_{os})_1$ is defined as

$$(\vec{k}_{os})_1 = [(\vec{k}_o)_1 + (\vec{k}_s)_1] / |(\vec{k}_o)_1 + (\vec{k}_s)_1|$$

and has a direction midway between the vector $(\vec{k}_o)_1$ and $(\vec{k}_s)_1$. In Figure 10, the first and second stages of the microscope are illustrated along with the associated nomenclature.

For electron waves encountered in the first stage, the atomic elastic scattering factor is given by the Born approximation as[8]

$$|f(\vec{s}_1)| = (2me^2/\hbar^2 s_1^2)[Z - F(s_1)]. \tag{3}$$

For a sample of identical subject atoms, the intensity recorded on the flat photographic plate through a rotating sector is

$$I(\vec{b}_2) = K\Phi(\vec{b}_2)|f(\vec{s}_1)|^2 \cos^3\phi / L^2 \tag{4}$$

where K is an experimental constant and is unimportant in the present treatment, L is the distance from the center point of the photographic plate (the hologram) to the origin of the scattered electron waves, $\vec{b}_2$ is the position on the hologram in relation to its center and $\Phi(\vec{b}_2)$ is the sector function. Substituting (3) into (4), one obtains

$$I(\vec{b}_2) = ZK(2me^2/\hbar^2)(\Phi\cos^3\phi/L^2 s_1^4)\{[Z - F(\vec{s}_1) - F^*(\vec{s}_1)] + |F(\vec{s}_1)|^2/Z\} \tag{5}$$

where $F(\vec{s}_1)$ is treated as a complex quantity. Since a flat plate is used to record the scattered electron waves, the recorded intensity as a function of $\vec{b}_2$ diminishes by $1/L^2\sec^3\phi$ and not $1/L^2$. Therefore, if one were to record data with a sector whose angular opening was proportional to $s_1^4\sec^3\phi$ the preceding equation may be rewritten as

$$I(\vec{b}_2) = K'[Z - F(\vec{s}_1) - F^*(\vec{s}_1)] \tag{6}$$

where

$$K' = ZK(2me^2/\hbar^2)^2(1/L^2)$$

and where the $|F(\vec{s}_1)|^2/Z$ term has been neglected. The term analogous to $|F(\vec{s}_1)|^2/Z$ is customarily neglected in conventional holography. The term does have the effect of distorting the reconstructed image somewhat, however.

A light wave that is transmitted through the hologram suffers a complex phase shift, $x(\vec{b}_2)$, given by the expression

$$x(\vec{b}_2) = n(\vec{b}_2) + iu(\vec{b}_2) \tag{7}$$

where $n(\vec{b}_2)$ is the phase shift due to the index of refraction of the hologram and $u(\vec{b}_2)$ expresses the attenuation of light by the blackening of the emulsion at $\vec{b}_2$. In the current treatment, $n(\vec{b}_2)$ is a constant which may be taken as zero and $u(\vec{b}_2)$ is related to the intensity of the scattered electrons by a constant, $K_u$, such that, neglecting nonlinearity in the emulsion response,

$$u(\vec{b}_2) = K_u[Z - F(\vec{s}_1) - F^*(\vec{s}_1)]. \tag{8}$$

The scattering factor, $G(\vec{s}_2)$, associated with the passage of a plane light wave, $A\exp(ik_2z)$, through the hologram can, for small angles, be expressed as [9]

$$\begin{aligned} G(\vec{s}_2) &= (-ik_2/2\pi)\int\exp(i\vec{s}_2\cdot\vec{b}_2)\{\exp[ix(\vec{b}_2)] - 1\}d^2\vec{b}_2 \\ &\approx (k_2K_u/2\pi)\int\exp(i\vec{s}_2\cdot\vec{b}_2)[u(\vec{b}_2)]d^2\vec{b}_2 \qquad (9) \\ &= C\int\exp(i\vec{s}_2\cdot\vec{b}_2)[Z - F(\vec{s}_1) - F^*(\vec{s}_1)]d^2\vec{b}_2 \\ &= F_{ref} + F_{subj} \qquad (10) \end{aligned}$$

where

$$C = k_2K_u/2\pi.$$

In this expression, $F_{ref}$ is the above integral with only the constant Z component and $F_{subj}$ is the remaining part which contains $F(\vec{s}_1)$ and $F^*(\vec{s}_1)$. All integration is over the region in which $\vec{b}_2$ ranges (the area of the hologram).

For small angles, the radial vector, $\vec{R}$, in the plane of the detector receiving the reconstructed waves in the second stage of the microscope is

$$\vec{R} = -(L_2/k_2)\vec{s}_2.$$

The scattering factor of the reconstructed subject wave, $F_{subj}(\vec{R})$, in stage 2 as a function of $\vec{R}$ may be obtained by substituting (1) into (10) and equating $\vec{b}_2$ as

$$\vec{b}_2 \approx -(L_1/k_1)\vec{s}_1.$$

The result may be expressed as

$$\begin{aligned} F_{subj}(\vec{R}) &= C\int \exp[i(k_2L_1/L_2k_1)\vec{R}\cdot\vec{s}_1] \\ &\quad \times[-F(\vec{s}_1) - F^*(\vec{s}_1)]\, d^2\vec{s}_1 \\ &= C\int \exp[i(\vec{R}/M)\cdot\vec{s}_1]\{\int \rho^p(\vec{b}_1)[-\exp(i\vec{s}_1\cdot\vec{b}_1) \\ &\quad - \exp(-i\vec{s}_1\cdot\vec{b}_1)]\, d^2\vec{b}_1\}\, d^2\vec{s}_1 \end{aligned} \tag{11}$$

where

$$\begin{aligned} M &= L_2k_1/L_1k_2 \\ &= L_2\lambda_2/L_1\lambda_1. \end{aligned}$$

In (11), the integration is over the entire domain of $\vec{s}_1$ (the range of recorded data) and $\vec{b}_1$ (the area of the hologram). Equation (11) may be rewritten in the following manner:

$$\begin{aligned} F_{subj}(\vec{R}) &= C\iint \exp[i(\vec{R}/M)\cdot\vec{s}_1]\exp(i\vec{s}_1\cdot\vec{b}_1) \\ &\quad \times\rho^p(\vec{b}_1)\, d^2\vec{b}_1 d^2\vec{s}_1 \\ &\quad + C\iint \exp[i(\vec{R}/M)\cdot\vec{s}_1]\exp(-i\vec{s}_1\cdot\vec{b}_1) \end{aligned}$$

$$x\rho^{P}(\vec{b}_1)d^2\vec{b}_1 d^2\vec{s}_1. \qquad (12)$$

For the purpose of the current work, the Fourier integral theorem can be expressed as [10]

$$\rho^{P}(\vec{b}') = (1/2\pi)\iint \exp(i\vec{b}'\cdot\vec{s})\exp(-i\vec{s}.\vec{b})\rho^{P}(\vec{b})d^2\vec{b}d^2\vec{s} \qquad (13)$$

where integration is over the entire domain of s and b. Therefore (11) is (neglecting the limited range of $\vec{s}_1$)

$$F_{subj}(\vec{R}) = 2C\pi[\rho^{P}(\vec{R}/M) + \rho^{P}(-\vec{R}/M)] \qquad (14)$$

This corresponds to the superposition of two reconstructed images; one is the projection of the original subject and the other the same but inverted. These projections have been magnified by the factor $M = L_2\lambda_2/L_1\lambda_1$. In the present work, these reconstructed images correspond to the real and virtual images formed by Fresnel diffraction patterns in conventional holography. In the present case, the diffraction patterns are all recorded at the Frauenhoffer limits. Furthermore, the atoms are, of course, spherical so that the two images are identical and exactly superposed on top of each other.

The intensity of the reconstruction is proportional to the square of $F_{subj}(\vec{R})$. Thus the observed intensity, neglecting distortions and integral termination effects due to the fact that $\vec{b}_2$ remains finite, is proportional to the square of the projected electron density. In Figure 11, a plot of $\log_{10}[\rho^{P}(b)/\rho^{P}(0)]^2$ versus b is drawn for neon and argon. The graph was plotted of densities computed from the atomic wave functions of Clementi and Raimondi based on Slater type wave functions.[11] The numerical integrations

required in the calculations were carried out on an IBM 360 computer.

Measurements made on photographs of the reconstructed atomic images indicate the region emphasized is in the vicinity of the L shell. The images in the current work fade beyond 0.28 Å for neon and 0.17 Å for argon. A limitation of this general magnitude is to be expected in view of the fact that the range of the sector ($5.9\ Å^{-1} < s < 40.1\ Å^{-1}$) restricts one to the region in which the contribution of the L shell to F(s) is well characterized but in which information on the K shell (available at large s values) and M shell (available at at small s values) is minimal. Furthermore argon appears roughly half as large as neon in Figure 8 because the atomic number of argon is almost twice that of neon.

The overall magnification, $M_{total}$, of the entire system (including subsequent enlargement) observed in Figure 8 is given as

$$M_{total} = (L_2\lambda_2/L_1\lambda_1)(R_H D_c/D_E)M_E. \qquad (15)$$

In this equation, $L_2\lambda_2/L_1\lambda_1$ is the same as before, $R_H$ is the factor by which the hologram was reduced for use in the laser diffractometer, $D_c$ is the focal length of the camera used to record the image of the reconstructed atom, $D_E$ is the focal length of the microscope eyepiece for the viewing of the image produced by the laser diffractometer and $M_E$ is the magnification due to enlarging the original photograph of the atom.

The optimal resolving power of this electron-holographic microscope can be calculated using the Abbe criterion for a microscope.[12] A formal statement of this rule as it applies to the current treatment for the microscope is

$$\delta = \lambda/2\sin\phi_m \qquad (16)$$

where $\lambda$ is the wavelength of the electron waves used to make the hologram and $\phi_m$ is the maximum value of the scattering angle in the first stage of the microscope. In the current experiment, $\lambda$ and $\phi_m$ have values of .06 Å and .38 respectively. Therefore the optimal resoving power is 0.08 Å. It is in (16) that the enormous advantage of holography over the conventional microscopy can be seen at once. Since no objective lens is required in holography, it is possible to exploit the comparitively large values of $\phi_m$ that can be attained easily. In electron microscopy, lens abberations are so severe that small numerical apertures are required, dictating values of $\phi_m$ between 1 and 2 orders of magnitude smaller than those used in holography.

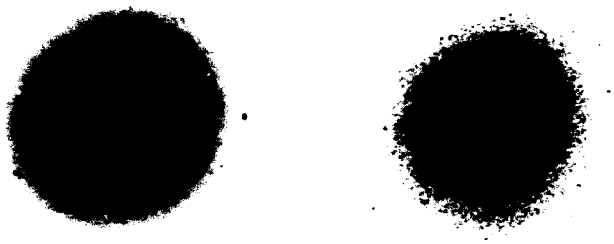


Figure 8 Reconstructed images of neon (left) and argon obtained from the second stage of the electron holographic microscope.

Figure 9 Schematic illustration of the laser-optical diffractometer a) He-Ne laser, b) -8.6 mm focal length diverging lens, c) 3 inch diameter, 45 inch focal length positive lens, d) hologram, e) microscope objective of 14 mm focal length.

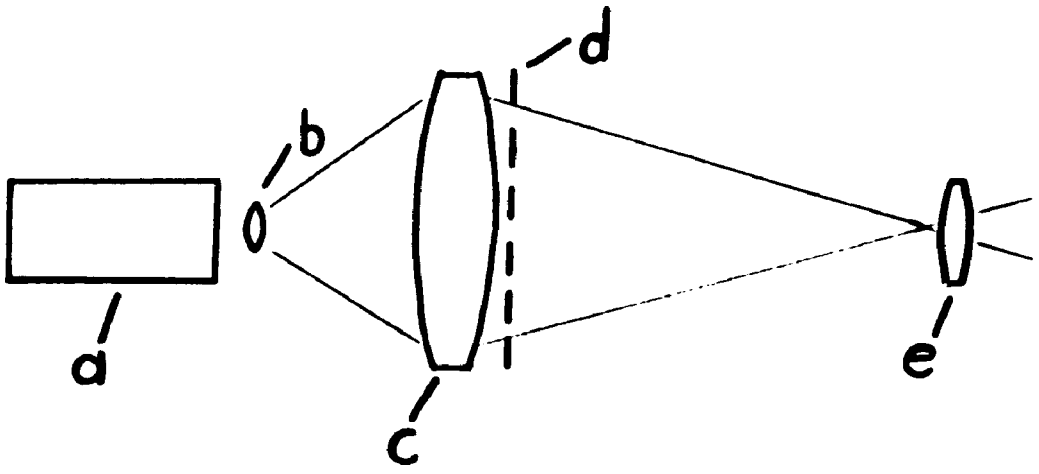

a
b
c
d
d
e

Figure 10 Schematic illustration of the first and second stages of the electron-holographic microscope and where

$\vec{b}_1$ = "impact parameter" of first stage

$(\vec{k}_o)_1$ = wave vector of incident electron waves in the first stage

$(\vec{k}_s)_1$ = wave vector of scattered electron waves in the first stage

$\vec{s}_1 = (\vec{k}_o)_1 - (\vec{k}_s)_1$

= scattering angle of electron waves in the first stage

$\vec{b}_2$ = the vector from the origin to any point in the plane of the hologram

$(\vec{k}_o)_2$ = wave vector of incident photon waves in the second stage

$(\vec{k}_s)_2$ = wave vector of scattered photon waves in the second stage

$\vec{s}_2 = (\vec{k}_o)_2 - (\vec{k}_s)_2$

$\vec{R}$ = the vector from the origin to any point in the plane of the reconstructed image.

$L_1$ = camera distance of the first stage

$L_2$ = distance of hologram from point of focus in the second stage.

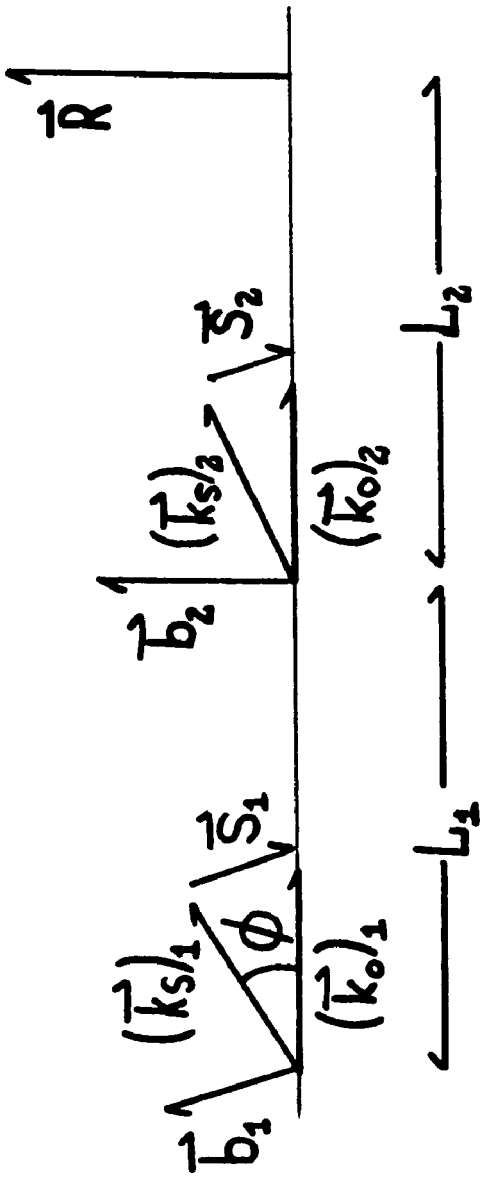
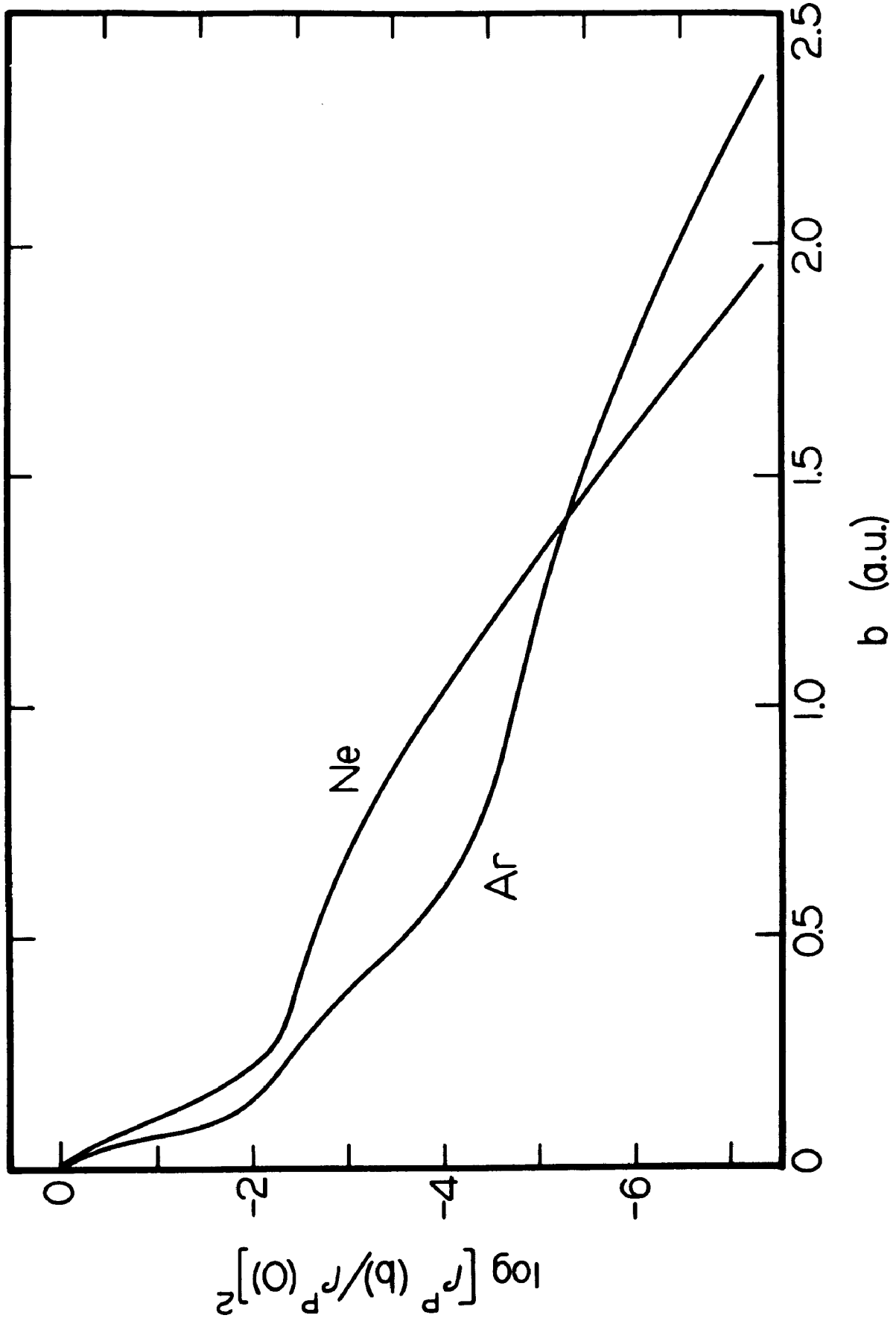

R
$\vec{S}_2$
$(\vec{k}_s)_2$
$(\vec{k}_o)_2$
$\vec{b}_2$
$L_2$
$\vec{S}_1$
$\phi$
$(\vec{k}_s)_1$
$(\vec{k}_o)_1$
$\vec{b}_1$
$L_1$

Figure 11 $\mathrm{Log}_{10}[\rho^{p}(b)/\rho^{p}(b)]^{2}$ versus b, the impact parameter.


log [r^P (b)/r^P (0)]^2
0
-2
-4
-6
0
0.5
1.0
1.5
2.0
2.5
b (a.u.)
Ne
Ar

## REFERENCES

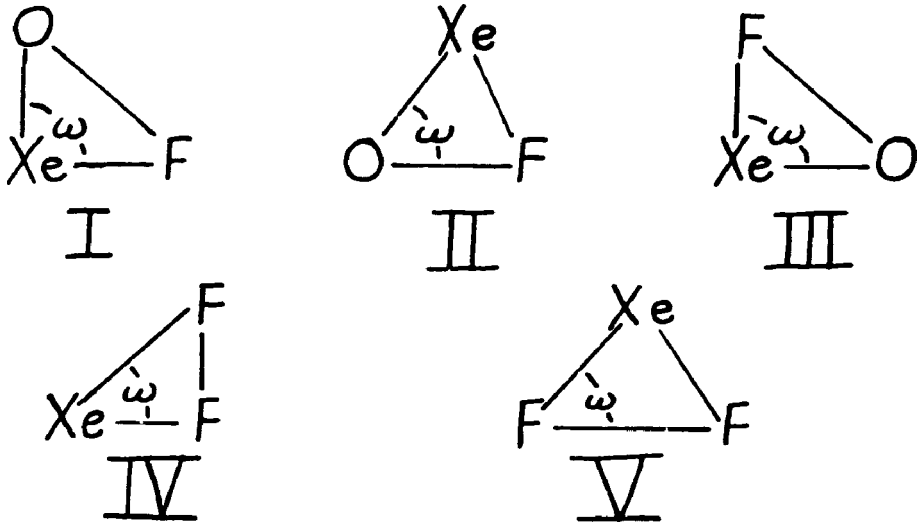
## PART II


1. D. Gabor, Nature, 161, 777(1948).
2. M. E. Haine and J. Dyston, Nature, 166, 315(1950); M. E. Haine and T. Mulvey, J. Opt. Soc., 42, 763(1952).
3. D. Gabor, Proc. Phys. Soc., 64, 449(1951).
4. L. S. Bartell, K. Kuchitsu and R. J. De Neui, J. Chem. Phys., 35, 1211(1961).
5. Kodak Publication No. P-116, 'Kodak Electron Image Plates', Eastman Kodak Company, Rochester, New York, 14650.
6. H. L. Lipson, 'Optical Transforms', Academic Press, London, 1972, p. 22.
7. R. G. Newton, 'Scattering Theory of Waves and Particles', Mc Graw-Hill, New York, 1966, p. 582.
8. For a discussion of the validity of the Born approximation see N. F. Mott and H. S. W. Massey, 'The Theory of Atomic Collisions', Third Edition, Oxford University Press, Oxford, 1965, pp. 464-6.
9. R. G. Newton, Op. Cit., p. 69.
10. H. Margenau and G. M. Murphy, 'The Mathematics of Physics and Chemistry', Second Edition, D. Van Nostrand Company, Princeton, 1956, pp. 252-4.
11. E. Clementi and D. L. Raimondi, J. Chem. Phys., 38, 2686(1963); E. Clementi, Phys. Rev., 127, 1618(1962).
12. M. Born and E. Wolf, 'Principles of Optics', Fourth

Edition, Pergamon Press, Oxford, 1970, p. 419.

## APPENDIX

The configurations used to calculate the multiple scattering corrections for $XeOF_4$ are shown in the following diagram.




For the purposes of comparison to the previous $XeOF_4$ structure study, the sine component of the multiple scattering correction was suppressed for configurations I and III since $\omega$ so nearly equals $90^{\circ}$. However, during the least squares refinement of the intensity data, no configuration was allowed to have its sine component suppressed.

For $XeOF_4$ as well as $ReF_6$ and $Pt(PF_3)_4$, the paralell amplitude of vibration presented in the three atom intensity equation was set equal to zero. This expediency resulted in no significant error since the $l_{\parallel}^2 s^2 \epsilon(s)$ term is normally small and on the order of one part per 100 or less. The more important $l_{\perp}$ term was always approximated by the

following non-rigorous expression:

$$l_{\perp} = l_{jk}\sin\omega_{ijk} + r_{jk}\cos\omega_{ijk}(\Delta\omega_{ijk})$$

where

$$\Delta\omega = (1/r_{jk}r_{ij}\sin\omega_{ijk})\{(r_{jk}^2 - r_{ij}^2 + r_{ik}^2)l_{jk}/r_{jk} + (r_{ij}^2 - r_{jk}^2 + r_{ik}^2)l_{ij}/r_{ij} - 2r_{ik}l_{ik}\}.$$